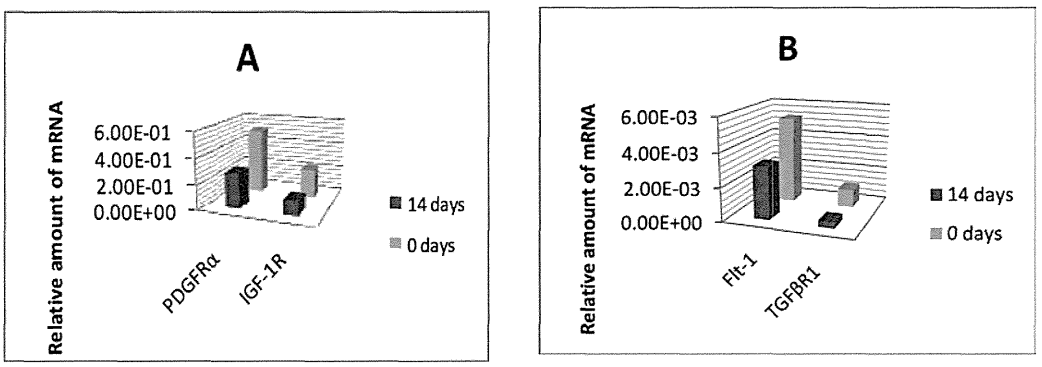

Fig. 5 Overall decrease in average expression of mRNA for PDGFRα and IGF-1R (A) and for Flt-1 and TGFβR1 (B) from day 0 to day 14 of consolidation (by quantitative real-time RT-PCR). GAPDH was used for a control; the amount of receptors' mRNA expression was calculated in relation to expression for GAPDH.

DISCUSSION

Growth factors are indispensible during any bone formation e.g., skeleton growth,[21,22] fracture healing[8] or callotasis,[20,23] or development of pathologic bone.[24] They control all stages of osteogenesis[25] including mesenchymal cell chemotaxis,[26] osteoprogenitor differentiation and proliferation,[22] matrix apposition, mineralization and remodeling,[23] and osteogenesis-related angiogenesis.[11,27] Growth factors or growth-factors-rich PRP accelerate the consolidation of distraction gaps,[4-7] bone cyst healing,[28] incorporation of bone grafts[29,30] and osteogenic differentiation of bone marrow.[3] Higher concentrations of PRP (GFs) have even superior impacts on bone formation.[31] VEGF, TGFβ, IGF and PDGF are obligatory for osteogenesis and are particularly abundant in PRP thus easily available. Therefore, receptors for these four growth factors became the scope of our investigation.

Since it was not feasible to examine receptors' mRNA in the four callus' zones individually, it posed a serious limitation to this study. However, consistently with the tissue-specific immunohistological examination, the mRNA analysis served to prove the overall drop in receptors' activity. Another limitation of this study was the semiquantitative evaluation of immunohistochemical staining. The cell count was subjective, and only randomly selected sections were evaluated. Moreover, no reasonable control could be designed (neither fracture healing nor healthy bone provides a sufficient fibrous zone or zone of rapid osteogenic changes for comparison). Such a selectivity of material, subjectivity of analysis and lack of control could not provide sound basis for a statistical analysis. However, semiquantitative analysis is a recommended method for the evaluation of cellular components,[18-20,32] and it allows observations of temporal changes in receptors' profiles and permits discussion of their clinical significance. We concluded that our results might at least provide a valuable indication for an improvement of distraction osteogenesis.

The initiation and sustaining of a distraction callus formation requires the vessels' development, in which osteogenesis follows angiogenesis. The inhibition of an Flt1 tyrosine kinase domain gene or the receptor itself reduces skeletal development.[11] We have found Flt1 in all callus regions, confirming its uniform involvement. Cells lining the new trabeculae expressed an exceptionally strong VEGF dependence. Flt 1 remained mild to moderate, especially in the woven and the trabecular tissue through the experiment, what was similar to findings in an early consolidation of a distracted mandible.[18]

TGFβ is stored in platelets, bone and cartilage. It guides mesenchymal cells and osteo-/chondroblasts towards the formation of mineralized, mature bone.[4,16] Endochondral and intramembranous ossification involve all isoforms of TGFβ receptor,[21] and only the interaction of TGFβ receptors I and II promotes bony tissue turnover.[15,17] During distraction osteogenesis, a vigorous proliferous activity is dependent upon TGFβR1.[33] In our experiment the woven and trabecular zones stained positively for TGFβR1 with only a slight decrease through consolidation. Such prolonged sensitivity, however, applied only to zones already differentiated towards bone. In contrast, TGFβR1 decreased early in the fibrous zone. That may imply an early loss of pro-osteogenic (consolidation) potential soon after an active distraction is terminated.

IGF is the most abundant growth factor stored in a bone matrix. Its cascade is activated in all rapidly growing tissues, it stimulates pro-osteogenic activity[19] and mediates mechanical stress effects.[23] It appears that the receptor itself has a greater regulatory effect than its ligand: IGF-R1 null mutation, IGF-R1 antibody,[13] and age related reduction of IGF-1R[14] all impair the pro-osteogenic effect. At the end of distraction we found abundant IGF-R1, especially in the osteoblasts. In distraction osteogenesis IGF-R1 is limited to bone of rich histology[33] (a low proliferation rate during impaired bone formation provokes abundant IGF activity and thus receptor down-regulation). We also found a weak though persistent IGF-R1 expression in fibrous tissue. Currently there is a growing interest in IGF binding proteins, which complicates the interpretation of the ligand-receptor signaling axis.

PDGF is an ideal initiator of a wound healing. It presents in the first hours after osteotomy and remains active until the late stages of bone formation.[25] During consolidation, PDGF is stored in all cells and matrix components.[32] PDGFRα transduces potent mitogenic signals[8] and exerts an antiapoptotic effect.[10] It is present in rapidly forming heterotrophic and osteophytic bone[24] and during fracture healing.[26] We, for the first time, confirmed the participation of PDGFRα in distraction osteogenesis. In cell cultures, the expression of the receptor declines after cells maturation.[34] Since PDGF may suppress osteogenic transformation, it is reasonable that we also found an initially very high PDGFRα participation reducing in an already formed bone (trabecular or woven). However, its rapid reduction in the fibrous zone (as seen in our study) may lead to an insufficient number of precursors ready for further osteogenic differentiation promoted by other growth factors.

Late bone formation in the distracted callus occurs through at least two mechanisms – central and peripheral. In the center, the pluripotential cells of the fibrous zone undergo osteogenic differentiation. In the periphery, the trabeculae provide an actively proliferating front of osteogenesis with pre-/ and osteoblasts invading the fibrous zone and replacing it. It seems that as soon as an active distraction is stopped, the decreased ability of the fibrous zone to respond to the pro-osteogenic factors (early decrease of receptors) may reduce central osteogenesis. During late consolidation, although receptors in the trabecular zone are preserved to some extent, growth factors seem to primarily stimulate bone maturation but no longer proliferation (a rich net of actively proliferating osteoblasts is replaced by sparsely distributed mature osteocytes). The trabecular zone loses its potential to invade the fibrous zone. Thus, both the central and peripheral consolidations decelerate. Replacement of the fibrous tissue may fail, and gap consolidation may be inefficient.

A predominantly fibrous distraction callus is encountered in various clinical situations: in congenital pseudoarthrosis, tumors, after irradiation, in osteoporotic bone, in various musculoskeletal dysplasiae and in case of an inadequate rate of distraction. A prolonged presence of a fibrous gap is one of the most serious concerns during bone lengthening and may have dramatic consequences. Thus, particularly in a poorly forming fibrous callus, a timely administration of growth factors seems to be imperative. This study shows that the callus' receptors are elevated

shortly after the termination of distraction and may provide a good target for exogenous growth factors. Therefore administration of growth factors into the distraction gap at this point should be the most beneficial, especially for promoting an early osteoinduction within the fibrous zone. During the later consolidation it might be more difficult to enhance osteogenesis with growth factors alone, as the number of target cells (carrying the specific receptors) decreases. However the behavior of receptors after growth factor injection is unforeseeable. For example their down regulation might occur. Further studies are warranted to examine receptors' response to exogenous growth factors. It would be essential to compare the rates of callus maturation when enhanced, with growth factors administered early or late during consolidation.

REFERENCES

1) Paley D: Problems, obstacles, and complications of limb lengthening by the Ilizarov technique. *Clin Orthop Relat Res*, 1990; 250: 81–104.
2) White SH, Kenwright J: The timing of distraction of an osteotomy. *J Bone Joint Surg Br*, 1990; 72: 356–361.
3) van den Dolder J, Mooren R, Vloon AP, Stoelinga PJ, Jansen JA: Platelet-rich plasma: quantification of growth factor levels and the effect on growth and differentiation of rat bone marrow cells. *Tissue Eng*, 2006; 12: 3067–3073.
4) Ozkan K, Eralp L, Kocaoglu M *et al*: The effect of transforming growth factor beta1 (TGF-beta1) on the regenerate bone in distraction osteogenesis. *Growth Factors*, 2007; 25: 101–107.
5) Robiony M, Polini F, Costa F, Politi M: Osteogenesis distraction and platelet-rich plasma for bone restoration of the severely atrophic mandible: preliminary results. *J Oral Maxillofac Surg*, 2002; 60: 630–635.
6) Swennen GR, Schutyser F, Mueller MC, Kramer FJ, Eulzer C, Schliephake H: Effect of platelet-rich-plasma on cranial distraction osteogenesis in sheep: preliminary clinical and radiographic results. *Int J Oral Maxillofac Surg*, 2005; 34: 294–304.
7) Kitoh H, Kitakoji T, Tsuchiya H, Katoh M, Ishiguro N: Transplantation of culture expanded bone marrow cells and platelet rich plasma in distraction osteogenesis of the long bones. *Bone*, 2007; 40: 522–528.
8) Tsiridis E, Upadhyay N, Giannoudis P: Molecular aspects of fracture healing: which are the important molecules? *Injury*, 2007; 38 Suppl 1: S11–25.
9) Tallquist M, Kazlauskas A: PDGF signaling in cells and mice. *Cytokine Growth Factor Rev*, 2004; 15: 205–213.
10) Heldin CH, Westermark B: Mechanism of action and in vivo role of platelet-derived growth factor. *Physiol Rev*, 1999; 79: 1283–1316.
11) Jacobsen KA, Al-Aql ZS, Wan C *et al*: Bone formation during distraction osteogenesis is dependent on both VEGFR1 and VEGFR2 signaling. *J Bone Miner Res*, 2008; 23: 596–609.
12) Otomo H, Sakai A, Uchida S *et al*: Flt-1 tyrosine kinase-deficient homozygous mice result in decreased trabecular bone volume with reduced osteogenic potential. *Bone*, 2007; 40: 1494–1501.
13) Wang Y, Nishida S, Boudignon BM *et al*: IGF-I receptor is required for the anabolic actions of parathyroid hormone on bone. *J Bone Miner Res*, 2007; 22: 1329–1337.
14) Cao JJ, Kurimoto P, Boudignon B, Rosen C, Lima F, Halloran BP: Aging impairs IGF-I receptor activation and induces skeletal resistance to IGF-I. *J Bone Miner*, Res 2007; 22: 1271–1279.
15) Steinbrech DS, Mehrara BJ, Rowe NM *et al*: Gene expression of TGF-beta, TGF-beta receptor, and extracellular matrix proteins during membranous bone healing in rats. *Plast Reconstr Surg*, 2000; 105: 2028–2038.
16) Derynck R, Feng XH: TGF-beta receptor signaling. *Biochim Biophys Acta*, 1997; 1333: F105–150.
17) Yamashita H, Ten Dijke P, Heldin CH, Miyazono K: Bone morphogenetic protein receptors. *Bone*, 1996; 19: 569–574.
18) Byun JH, Park BW, Kim JR, Lee JH: Expression of vascular endothelial growth factor and its receptors after mandibular distraction osteogenesis. *Int J Oral Maxillofac Surg*, 2007; 36: 338–344.
19) Haque T, Amako M, Nakada S, Lauzier D, Hamdy RC: An immunohistochemical analysis of the temporal and spatial expression of growth factors FGF 1, 2 and 18, IGF 1 and 2, and TGFbeta1 during distraction osteogenesis. *Histol Histopathol*, 2007; 22: 119–128.
20) Tavakoli K, Yu Y, Shahidi S, Bonar F, Walsh WR, Poole MD: Expression of growth factors in the mandibular

distraction zone: a sheep study. *Br J Plast Surg*, 1999; 52: 434–439.
21) Horner A, Kemp P, Summers C *et al*: Expression and distribution of transforming growth factor-beta isoforms and their signaling receptors in growing human bone. *Bone*, 1998; 23: 95–102.
22) Sakou T, Onishi T, Yamamoto T, Nagamine T, Sampath T, Ten Dijke P: Localization of Smads, the TGF-beta family intracellular signaling components during endochondral ossification. *J Bone Miner Res*, 1999; 14: 1145–1152.
23) Weiss S, Baumgart R, Jochum M, Strasburger CJ, Bidlingmaier M: Systemic regulation of distraction osteogenesis: a cascade of biochemical factors. *J Bone Miner Res*, 2002; 17: 1280–1289.
24) Horner A, Bord S, Kemp P, Grainger D, Compston JE: Distribution of platelet-derived growth factor (PDGF) A chain mRNA, protein, and PDGF-alpha receptor in rapidly forming human bone. *Bone*, 1996; 19: 353–362.
25) Chaudhary LR, Hofmeister AM, Hruska KA: Differential growth factor control of bone formation through osteoprogenitor differentiation. *Bone*, 2004; 34: 402–411.
26) Fujii H, Kitazawa R, Maeda S, Mizuno K, Kitazawa S: Expression of platelet-derived growth factor proteins and their receptor alpha and beta mRNAs during fracture healing in the normal mouse. *Histochem Cell Biol*, 1999; 112: 131–138.
27) Weiss S, Zimmermann G, Baumgart R, Kasten P, Bidlingmaier M, Henle P: Systemic regulation of angiogenesis and matrix degradation in bone regeneration–distraction osteogenesis compared to rigid fracture healing. *Bone*, 2005; 37: 781–790.
28) Cieslik-Bielecka A, Bielecki T, Gazdzik TS, Cieslik T, Szczepanski T: Improved treatment of mandibular odontogenic cysts with platelet-rich gel. *Oral Surg Oral Med Oral Pathol Oral Radiol Endod*, 2008; 105: 423–429.
29) Marx RE: Platelet-rich plasma: evidence to support its use. *J Oral Maxillofac Surg*, 2004; 62: 489–496.
30) Marx RE, Carlson ER, Eichstaedt RM, Schimmele SR, Strauss JE, Georgeff KR: Platelet-rich plasma: Growth factor enhancement for bone grafts. *Oral Surg Oral Med Oral Pathol Oral Radiol Endod*, 1998; 85: 638–646.
31) Kawasumi M, Kitoh H, Siwicka KA, Ishiguro N: The effect of the platelet concentration in platelet-rich plasma gel on the regeneration of bone. *J Bone Joint Surg Br*, 2008; 90: 966–972.
32) Knabe C, Nicklin S, Yu Y *et al*: Growth factor expression following clinical mandibular distraction osteogenesis in humans and its comparison with existing animal studies. *J Craniomaxillofac Surg*, 2005; 33: 361–369.
33) Eingartner C, Coerper S, Fritz J, Gaissmaier C, Koveker G, Weise K: Growth factors in distraction osteogenesis. Immuno-histological pattern of TGF-beta1 and IGF-I in human callus induced by distraction osteogenesis. *Int Orthop*, 1999; 23: 253–259.
34) Yu X, Hsieh SC, Bao W, Graves DT: Temporal expression of PDGF receptors and PDGF regulatory effects on osteoblastic cells in mineralizing cultures. *Am J Physiol*, 1997; 272: C1709–1716.

Biochemical and Biophysical Research Communications 417 (2012) 1193–1199

Contents lists available at SciVerse ScienceDirect

Biochemical and Biophysical Research Communications

journal homepage: www.elsevier.com/locate/ybbrc

Mesenchymal stem cell isolation and characterization from human spinal ligaments

Toru Asari [a,b], Ken-Ichi Furukawa [b,*], Sunao Tanaka [a], Hitoshi Kudo [a], Hiroki Mizukami [c], Atsushi Ono [a], Takuya Numasawa [a], Gentaro Kumagai [a], Shigeru Motomura [b], Soroku Yagihashi [c], Satoshi Toh [a]

[a] Department of Orthopaedic Surgery, Hirosaki University Graduate School of Medicine, 5 Zaifu-cho, Hirosaki, Aomori 036-8562, Japan
[b] Department of Pharmacology, Hirosaki University Graduate School of Medicine, 5 Zaifu-cho, Hirosaki, Aomori 036-8562, Japan
[c] Department of Pathology and Molecular Medicine, Hirosaki University Graduate School of Medicine, 5 Zaifu-cho, Hirosaki, Aomori 036-8562, Japan

ARTICLE INFO

Article history:
Received 15 December 2011
Available online 27 December 2011

Keywords:
Mesenchymal stem cells
Spinal ligaments
Differentiation
Localization
Pathogenesis
Ectopic ossification

ABSTRACT

Mesenchymal stem cells (MSCs) have a fibroblast-like morphology, multilineage potential, long-term viability and capacity for self-renewal. While several articles describe isolating MSCs from various human tissues, there are no reports of isolating MSCs from human spinal ligaments, and their localization *in situ*. If MSCs are found in human spinal ligaments, they could be used to investigate hypertrophy or ossification of spinal ligaments. To isolate and characterize MSCs from human spinal ligaments, spinal ligaments were harvested aseptically from eight patients during surgery for lumbar spinal canal stenosis and ossification of the posterior longitudinal ligament. After collagenase digestion, nucleated cells were seeded at an appropriate density to avoid colony-to-colony contact. Cells were cultured in osteogenic, adipogenic or chondrogenic media to evaluate their multilineage differentiation potential. Immunophenotypic analysis of cell surface markers was performed by flow cytometry. Spinal ligaments were processed for immunostaining using MSC-related antibodies. Cells from human spinal ligaments could be extensively expanded with limited senescence. They were able to differentiate into osteogenic, adipogenic or chondrogenic cells. Flow cytometry revealed that their phenotypic characteristics met the minimum criteria of MSCs. Immunohistochemistry revealed the localization of CD90-positive cells in the collagenous matrix of the ligament, and in adjacent small blood vessels. We isolated and expanded MSCs from human spinal ligaments and demonstrated localization of MSCs in spinal ligaments. These cells may play an indispensable role in elucidating the pathogenesis of numerous spinal diseases.

1. Introduction

The ligaments surrounding the spine guide segmental motion and contribute to the intrinsic stability of the spine by limiting excessive motion [1]. Hypertrophy and ossification of the spinal ligaments can contribute to the narrowing of the spinal canal. This is seen in cases of lumbar spinal canal stenosis (LSCS), ossification of the longitudinal ligament (OPLL) and ossification of the ligamentum flavum (OLF) [2] and may cause spinal cord injury and myelopathy, with many patients suffering from various symptoms. Patients require drug treatment and in severe cases surgery may be required to decompress the spinal cord by removing spinal ligaments. Although the pathologies of these diseases are not fully understood at a cellular level, stem cells are believed to play an important role in their progression [3–5].

Mesenchymal stem cells (MSCs) have a fibroblast-like morphology, multilineage potential, long-term viability and a capacity for self-renewal [6,7]. They are phenotypically characterized by the expression of the cell surface markers [8]. MSCs can be isolated from various human tissues, and have many common features [6,7,9,10], however, many reports describe distinguishing characteristics that are dependent on their origin [12–14].

Although MSCs from various tissues have been used in regenerative medicine [15] and for elucidating the pathogenesis of numerous diseases in rats [3,4,16], there are no reports on the isolation of MSCs from human spinal ligaments and their localization *in situ*. We attempted to test the hypothesis that MSCs exist in human spinal ligaments and contribute to the pathogenesis of spinal diseases. If MSCs are found to exist in human spinal ligaments, they may be used to investigate the pathogenesis of hypertrophy or ossification of spinal ligaments. Additionally, understanding the localization of MSCs in human spinal ligaments may assist in future strategies to treat spinal diseases. Therefore, the purpose of this study was to isolate and characterize MSCs from human spinal ligaments.

2. Materials and methods

2.1. Clinical diagnosis and spinal ligament samples

Lumbar spinal canal stenosis or OPLL diagnosis was confirmed by X-ray, computed tomography and magnetic resonance imaging

* Corresponding author. Fax: +81 172 39 5023.
E-mail address: furukawa@cc.hirosaki-u.ac.jp (K.-I. Furukawa).

0006-291X/$ - see front matter © 2012 Elsevier Inc. All rights reserved.
doi:10.1016/j.bbrc.2011.12.106

of the spine. Spinal ligament samples were harvested aseptically from eight patients during surgery. Clinical diagnoses and features of samples used in this study are shown in Table 1 (No. 1–8).

2.2. Cell isolation and culture

Spinal ligament tissues were rinsed with phosphate-buffered saline (PBS) to remove blood and debris, and the surrounding tissue and calcification area were carefully removed under a dissection microscope. Collected ligaments were minced into 0.5 mm^3 pieces and washed twice with PBS, then digested using 3 mg/mL collagenase (Type 5; Sigma-Aldrich, St. Louis, MO, USA) in α-modified Eagle's medium (α-MEM; Invitrogen, Carlsbad, CA, USA) at 37 °C. After 3 h, digested tissue was filtered through a 70-μm nylon filter (BD Biosciences, San Jose, CA, USA) to remove debris. Nucleated cells were resuspended after centrifugation [10], and plated at densities of 1×10^4, 1×10^5, 5×10^5 or 1×10^6 cells/94-mm culture dish (Greiner Bio-One, Mosonmagyarovar, Hungary), in triplicate for each density. Cells were maintained in α-MEM supplemented with 10% fetal bovine serum (JRH Bioscience, Lenexa, KS, USA), 100 U/mL penicillin G sodium and 100 μg/mL streptomycin sulfate (Invitrogen). Cultures were incubated in a humidified atmosphere of 95% air and 5% CO_2 at 37 °C for 14 days at passage 0. After 14 days, a representative dish for each seeding density was stained with 0.5% crystal violet (Wako Pure Chemical Industries, Osaka, Japan). The optimal initial cell density was determined based on the following criteria [9]: (a) colony size was not affected by contact inhibition; and (b) the highest number of colonies obtained. From the two remaining dishes, the cells were detached with a solution of 0.02% EDTA and 0.05% trypsin, washed twice with conditioned medium, and centrifuged at 200*g* for 5 min. Cells were then counted to determine the number of cells at passage 0 and replated at a density of 50 cells/cm^2 in 94-mm dishes and cultured at subconfluent levels. Serial passaging of the cells was performed at the same density.

2.3. Colony-forming unit-fibroblast (CFU-F) assay

To test colony-forming efficiency [17], cells from passage 0 were replated at a density of 100 cells/94-mm dish in three dishes. After 14 days, colonies were visualized and counted after fixing in 4% formaldehyde followed by staining with 0.5% crystal violet in methanol for 5 min. Cells were washed twice in distilled water and the number of colonies per dish was determined. Aggregates of $\geqslant$50 cells were scored as colonies.

2.4. Cell proliferation assay

To examine cell proliferative ability [12], cells were replated at 50 cells/cm^2 every 14 days and at 5000 cells/cm^2 every 5 days. Cells were counted and replated at the same density until their expansion potential was lost. For each passage, we calculated population doubling (PD) using the formula $PD = \log_2 [Nc/N_0]$. N_0 is the inoculum cell population and Nc is the number of cells at confluence. The PD values from each passage were added together to obtain cumulative population doubling values.

Table 1
Clinical diagnosis, patient gender and age of tissue samples.

No.	Sex /Age	Diagnosis	Spinal ligament
1	F/62	LSCS	PLL
2	M/45	OPLL	LF
3	F/72	LSCS	LF
4	F/72	LSCS	LF
5	M/74	LSCS	LF
6	F/68	OPLL	LF
7	M/69	OPLL	PLL
8	M/71	OPLL	LF

M: male, F: female.
LF: ligamentum flavum; LSCS: lumbar spinal canal stenosis; OPLL: ossification of the posterior longitudinal ligament of the spine; PLL: posterior longitudinal ligament.

2.5. Flow cytometry

Approximately 1×10^6 cells from passages 1–3 were washed with PBS containing 2% FBS (washing buffer). Cells were resuspended in 50 μL PBS containing fluorochrome-conjugated mouse anti-human CD11b, CD19, CD34, CD45, CD73, CD90, CD105 and HLA-DR (Becton Dickson) monoclonal antibodies. Mouse monoclonal isotype antibodies were used to detect any non-specific fluorescence, following manufacturer's recommendations. After incubation in the dark for 40 min at 4 °C, cells were resuspended in 300 μL washing buffer. Cell fluorescence was evaluated using a FACSCanto™ II instrument (BD Biosciences); data were analyzed with CellQuest software (BD Biosciences).

2.6. Cell differentiation

For osteogenic differentiation, cells from passages 1–3 were replated at densities of 1×10^5 cells/94-mm dish for cytohistological staining, and 3×10^4 cells/35-mm dish for PCR analysis. They were cultured to subconfluent levels; osteogenic medium was then added for 21 days. Osteogenic medium consisted of conditioned medium supplemented with 1 nM dexamethasone (ICN Biomedicals Inc., Costa Mesa, CA, USA), 10 mM β-glycerol phosphate (Wako Pure Chemical Industries) and 50 μg/mL ascorbic acid (Wako Pure Chemical Industries), as previously reported [11]. To evaluate the mineralized matrix, cells were fixed in 4% formaldehyde for 10 min and stained with 1% Alizarin Red S (Sigma-Aldrich) for 10 min.

For adipogenic differentiation, cells from passages 1–3 were replated at densities of 1×10^5 cells/94-mm dish for cytohistological staining, and 3×10^4 cells/35-mm dish for PCR analysis. They were cultured to subconfluent levels; medium was then changed to adipogenic medium for 21 days. The adipogenic medium consisted of conditioned medium supplemented with 100 nM dexamethasone, 0.5 mM isobutylmethylxanthine (Wako Pure Chemical Industries) and 100 μM indomethacin (Sigma-Aldrich), as previously reported [18]. To evaluate droplet formation, cells were fixed in 4% formaldehyde for 5 min and stained with Oil Red O (Nacalai Tesque Inc., Kyoto, Japan) for 20 min.

For chondrogenic differentiation, 2×10^5 cells from passages 1–3 were centrifuged for 10 min at 450*g* in a 15-mL polypropylene tube. The pellet was then treated with chondrogenic medium for 21 days. Chondrogenic medium consisted of conditioned medium supplemented with 500 ng/mL bone-morphogenic protein 2 (R&D Systems, Minneapolis, MN, USA), 10 ng/mL transforming growth factor-β3 (R&D Systems) and 100 nM dexamethasone, as previously reported [10,19]. For microscopy, the pellet was fixed in 10% formaldehyde, dehydrated through serial ethanol dilutions and embedded in paraffin. Blocks were cut into 5-μm sections and stained with Toluidine Blue (KANTO Chemical Co., Inc., Tokyo, Japan).

2.7. Gene expression analysis

On 0, 7, 14, and 21 days, total RNA was extracted from differentiation-induced and uninduced cultured cells or cell pellets, using an RNeasy Mini Kit (QIAGEN, Valencia, CA, USA) according to the manufacturer's instructions [13]. First strand cDNA was synthesized from 1 μg of total RNA, using standard random hexamer priming techniques. Real-time polymerase chain reaction (PCR)

was carried out with Power SYBR Green PCR Master Mix on an ABI Prism® 7000 Sequence Detection System (Applied Biosystems, Foster City, CA, USA). Primers for the genes we examined were designed using Primer Express software (Applied Biosystems) as indicated in Table 2. Real-time PCR conditions and analysis was performed as previously described [20]. Graphs show relative expression levels compared with the control on day 0.

2.8. Immunohistochemical staining of spinal ligaments

Spinal ligaments from two patients (Table 1, No. 7 and 8) were fixed in 10% formaldehyde for 7 days at 4 °C. The samples were further decalcified for 4–7 days at room temperature in KC-X (Falma, Tokyo, Japan), embedded in paraffin, and cut into 4-μm sections. For immunohistochemical staining, serial 4-μm sections were deparaffinized with xylene, and treated with ethanol. After washing with PBS, endogenous peroxidases were blocked with 0.3% H_2O_2/methanol at room temperature for 10 min and then washed with PBS. Antigen retrieval was conducted using a PASCAL pressure chamber (DAKO Cytomation, Produktionsvej, Glostrup, Denmark) following the manufacturer's protocol. Sections were blocked with normal serum at room temperature for 30 min, then incubated with the following primary antibodies at 4 °C overnight: monoclonal anti-CD34 (diluted antibody; Ventana medical system Inc., Tucson, AZ, USA); monoclonal anti-CD45 (1:200; DAKO Cytomation); and monoclonal anti-CD90 (1:250; Abcam, Cambridge, MA, USA). Sections were incubated with secondary and tertiary agents from a streptavidin-biotin-peroxidase detection kit (Histofine SAB-PO Kit; Nichirei, Tokyo, Japan). *N,N′*-diaminobenzidine was used to visualize peroxidase deposition at the antigenic sites; these sections were lightly counterstained with hematoxylin. Specificity was confirmed by replacement of primary antibodies with non-immune sera or by omission of primary antibodies.

2.9. Statistical analysis

Expression levels of each mRNA are shown as mean ± standard error of the mean ($n = 6$). Mann-Whitney *U*-test was used to assess significant differences between cultured cells on each day vs the control on day 0, and between induced and uninduced groups on each day. $P \leqslant 0.05$ was considered statistically significant.

3. Results

3.1. In vitro expandability with limited senescence of human spinal ligament cells

Adherent cells appeared to be a relatively homogenous population of fibroblast-like and spindle-shaped cells (Fig. 1A). First, we determined the optimal initial density of nucleated cells that avoided colony-to-colony contact inhibition to be 5×10^5 cells/94-mm dish (Fig. 1B). Cells were replated at a density of 100 cells/94-mm dish to estimate their colony-forming efficiency. After 14 days, cells were stained with 0.5% crystal violet and single-cell-derived colonies were counted. Colony-forming efficiency was determined as 8.8 ± 6.8 colonies/100 cells plated. Data are shown as mean ± standard deviation of 18 plates.

To investigate *in vitro* expandability, cells were replated at a low density (50 cells/cm^2) every 14 days, and a high density (5000 cells/cm^2) every 4–5 days until their expansion potential was lost. The proliferative ability of the cells was retained even at a low density at passage 7. Population doubling was greater than 30 doublings for low-density cells and 10 doublings for high-density cells (Fig. 1C).

Table 2
Primer oligonucleotide sequences used for real-time PCR.

Gene	Forward primer 5′–3′	Reverse primer 5′–3′
G3PDH	TGCACCACCAACTGCTTAGC	GGCATGGACTGTGGTCATGAG
BMP2	AGATGAACACAGCTGGTCACAGA	GGAAGGATGCCCTTTTCCA
Runx2	GCCTTCAAGGTGGTAGCCC	CGTTACCCGCCATGACAGTA
ALP	ACGAGCTGAACAGGAACAACGT	CACCAGCAAGAAGAAGCCTTTG
PPARγ2	TGAATGTGAAGCCCATTGAA	CTGCAGTAGCTGCACGTGTT
LPL	ATGTGGCCCGGTTTATCA	CTGTATCCCAAGAGATGGACATT
Sox9	GTACCCGCACTTGCACAAC	TCGCTCTCGTTCAGAAGTCTC
COL2A1	CCGGGCAGAGGGCAATAGCAGGTT	CATTGATGGGGAGGCGTGAG
COL10A1	CATGTTTGGGTAGGCCTGTATAAGA	ACTCCCTGAAGCCTGATCCA

3.2. Immunophenotypic characterization of spinal ligament cells

Flow cytometric analysis showed positive expression for CD73, CD90 and CD105, and low or no expression of CD11b, CD19, CD34, CD45 and HLA-DR, indicating that cells derived from human spinal ligaments had MSC characteristics (Fig. 2). Mean surface immunophenotype expression values and standard deviations were as follows: CD11b (0.03 ± 0.05%), CD19 (0.08 ± 0.04%), CD34 (7.70 ± 7.17%), CD45 (0.20 ± 0.15%), CD73 (99.9 ± 0.08%), CD90 (100%), CD105 (99.9 ± 0.08%), and HLA-DR (0%).

3.3. In vitro differentiation into osteoblasts, adipocytes and chondrocytes

Cells treated with osteogenic medium for 21 days changed from a spindle-shaped morphology, and became broader as periods of osteogenic induction increased, forming a mineralized matrix, as shown by Alizarin Red S staining. Cells grown in control medium did not form a mineralized matrix. Real-time PCR showed that both induced and uninduced groups expressed osteogenesis-specific genes compared with the control on day 0. Expression levels in induced groups were always higher than in uninduced groups. Especially, the expression level of *Runx2* on day 21 in the induced group was significantly higher than in the control on day 0 and the uninduced group on day 21. *ALP* mRNA expression on day 21 was significantly higher in the induced group than in the control on day 0 (Fig. 3A).

The adipogenic potential of cells was assessed by treating with adipogenic medium for 21 days. Lipid vacuoles were noticeable as early as 7 days after adipogenic induction and visualized by staining with Oil Red O. There was no formation of lipid vacuoles in control medium. Expression of adipogenesis-specific genes was elevated not only in induced groups but also in uninduced groups compared with the control on day 0. However, expression levels in induced groups were always higher than in uninduced groups. Especially, *LPL* mRNA expression on each day was significantly higher in induced groups than in uninduced groups, and the control on day 0. *PPARγ2* mRNA expression on each day was significantly higher in induced groups than in the control on day 0; by day 21, it was significantly higher than in uninduced groups (Fig. 3B).

To evaluate chondrogenic potential, cell pellets were treated with chondrogenic medium for 21 days. The cell pellets treated with chondrogenic medium were morphologically smooth, with increased size due to production of extracellular matrix. Thin sections of the cell pellet displayed cartilage-specific metachromasia through Toluidine Blue staining after 21 days in chondrogenic medium. Expression of chondrogenesis-specific genes was elevated in both induced and uninduced groups compared with the control on day 0. Expression levels in induced groups were always higher than in uninduced groups. Especially, *Sox9* mRNA expression on day 14 was significantly higher in induced groups than in uninduced groups, and in the control on day 0. *COL10A1* mRNA

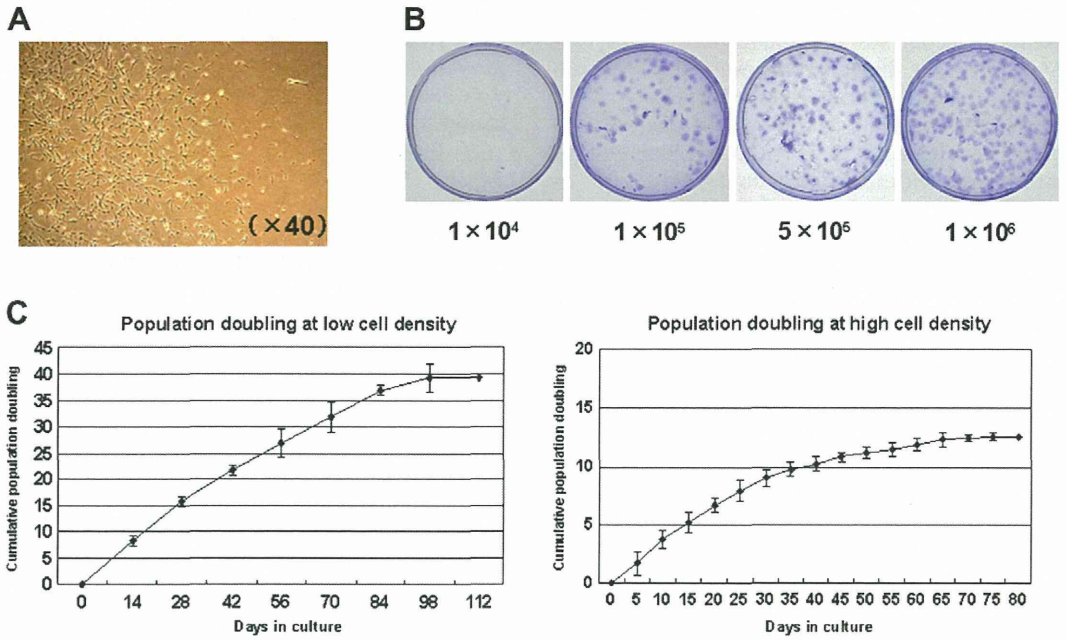

Fig. 1. (A) Phase-contrast views of cells from human spinal ligaments. Cells that adhered to plastic and formed colonies were fibroblast-like and spindle-shaped. (B) Colony formation of passage 0 cells seeded at various densities. The optimal cell density to avoid colony-to-colony contact while obtaining the most colonies was 5×10^5 cells/94-mm dish. (C) Proliferation potential of cells from human spinal ligaments. Passage 1 cells were replated at 50 cells/cm^2 (low density) every 14 days and at 5000 cells/cm^2 (high density) every 5 days until their expansion potential was lost. Values are means ± SD of samples from six donors (No. 1–6).

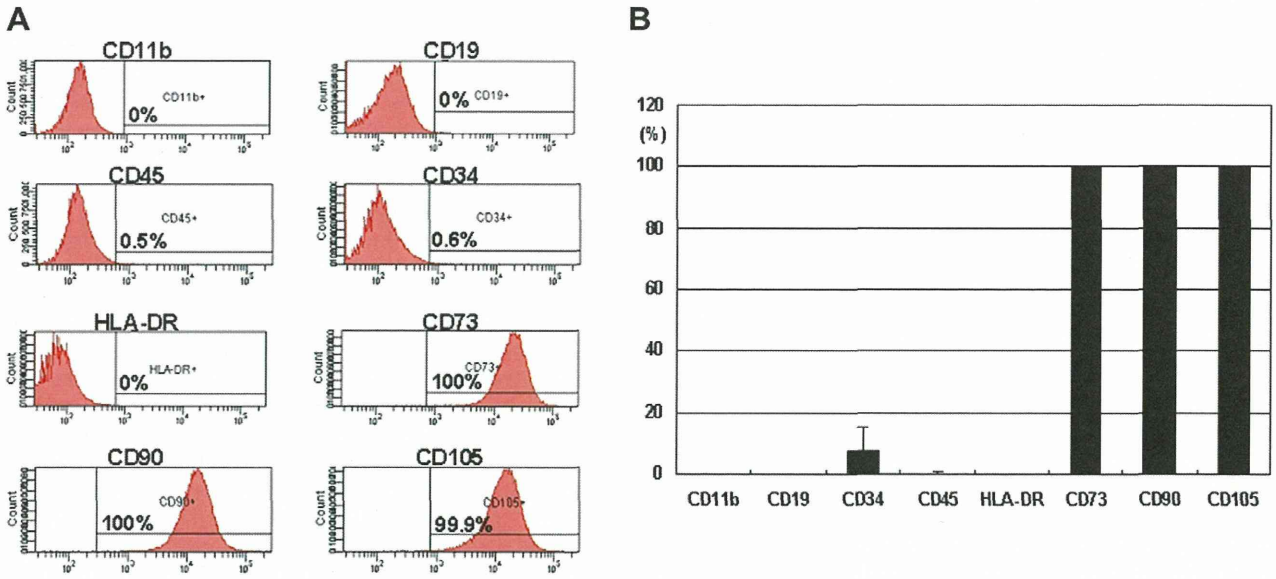

Fig. 2. Expression of stem cell-specific surface markers on cells isolated from human spinal ligaments. (A) A representative histogram of each surface marker. (B) Data are shown as mean ± SD of samples from six donors (No. 1–6).

expression on day 14 was significantly higher in induced groups than in uninduced group, and in the control on day 0 (Fig. 3c).

3.4. Immunohistochemical localization of MSCs within spinal ligaments

Spindle cells in collagenous matrix and adjacent small blood vessels within spinal ligaments (both ligamentum flavum and posterior longitudinal ligament) were positive for CD90. CD34$^+$ spindle-shaped cells were mainly observed in collagenous matrix and on vessels, but to a lesser extent than CD90. However, CD45$^+$ cells were not seen in all ligament tissues (Fig. 4). CD34 is generally expressed on endothelial cells of vessels and stromal cells, such as myofibroblasts, in addition to hematopoietic progenitor cells. In this case, CD34$^+$ cells could be stromal or endothelial cells. We did not see marked differences between ligamentum flavum and posterior longitudinal ligaments. Immunohistochemistry of spinal ligaments showed that MSCs may be ligament components, and may be associated with blood vessels.

4. Discussion

Many researchers have reported that MSCs can be isolated from various mesenchymal tissues [6,7,9,10]; MSCs from some tissues have already been used in clinical trials [15]. However, MSCs from human spinal ligaments and their localization *in situ* have not yet

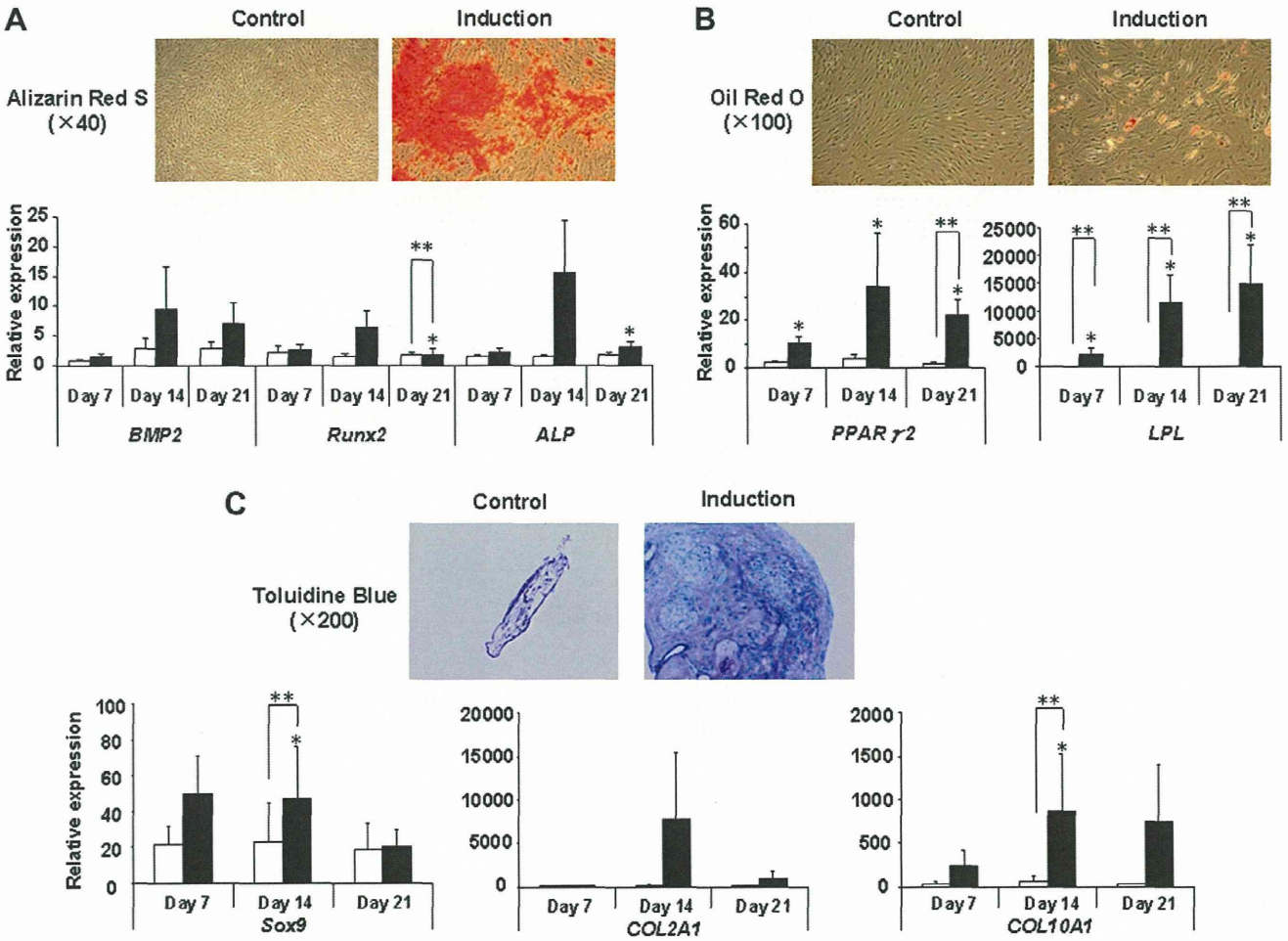

Fig. 3. Differentiation potentials of cells from human spinal ligaments. (A) Osteogenic differentiation. After cells were treated with osteogenic medium for 21 days, mineralization in treated cells was revealed by Alizarin Red S staining. (B) Adipogenic differentiation. After cells were treated with adipogenic medium for 21 days, lipid vacuoles were visualized by staining with Oil Red O. (C) Chondrogenic differentiation. After a cell pellet was treated with chondrogenic medium for 21 days, 5-μm sections of the cell pellet displayed cartilage-specific metachromasia with Toluidine Blue staining. The fold increase of each mRNA expression was compared with the control on day 0. Values are the mean ± SEM of samples from six donors (No. 1–6). Open and closed columns indicate uninduced group and induced group, respectively. *Significantly different from the control on day 0; $P \leqslant 0.05$. **Significantly different from uninduced group on each day; $P \leqslant 0.05$.

been reported. In this study, we isolated cells from human spinal ligaments that were fibroblast-like, could adhere to plastic, and could be substantially sub-cultured *in vitro*. We showed these cells to have high self-renewal capacity with limited senescence. Distribution of cell surface markers on these cells, as analyzed by flow cytometry, was similar to those previously reported in MSCs [8,10]. They could also be induced to differentiate into osteoblasts that produce mineralized matrix, adipocytes that accumulate lipid vacuoles, and chondrocytes that produce mucopolysaccharide, under appropriate conditions *in vitro*. Real-time PCR analysis showed that mRNA expression of genes involved in osteogenesis, adipogenesis, or chondrogenesis was elevated after induction compared with the control on day 0. Thus, we successfully demonstrated the existence of MSCs in spinal ligaments using previously reported methods [10,12]. MSCs could be obtained regardless of the patients' age, vertebral level and disease phenotype.

Mesenchymal stem cells isolated from various tissues share common features [21], such as clonogenic characteristics, multilineage differentiation and cell surface immunophenotypes, independent of their origin [6,7,9,10]. However, many reports describe significant differences in MSC properties depending on their origin [12–14]. In this study, MSCs from human spinal ligaments could be expanded *in vitro* for more than 30 population doublings at low densities, and approximately 10 doublings at high densities. We also showed that the self-renewal capacity of MSCs from human spinal ligaments was not less than other mesenchymal tissues, such as bone marrow, synovium, adipose tissue and knee muscle [12]. Expression levels of tri-lineage specific marker genes in induced groups were higher than in uninduced groups. However, even expression levels of uninduced groups were higher than those of the control on day 0. MSCs from human spinal ligaments might change their expression levels owing to spontaneous differentiation, or influence of long-term culture [22].

Localization of MSCs *in situ* is controversial; however, some researchers have reported that MSCs may exist in perivascular cells of various human tissues [23]. We demonstrated that spindle cells in collagenous matrix and in adjacent small blood vessels within spinal ligaments were positive for CD90, and partially positive for CD34. Recently, stem/progenitor cells have been identified in tendon extracellular matrix, suggesting that several extracellular matrix components are critical organizers of the stem cell niche [24]. Our immunohistochemistry results from human spinal ligaments agree with these reports.

Lumbar spinal canal stenosis is caused by hypertrophy of ligamentum flavum [25]; OPLL and OLF are caused by ossification of spinal ligaments [2]. Hypertrophy and ossification of spinal ligaments can contribute to narrowing of the spinal canal, and may cause symptoms indicative of spinal cord injury and myelopathy.

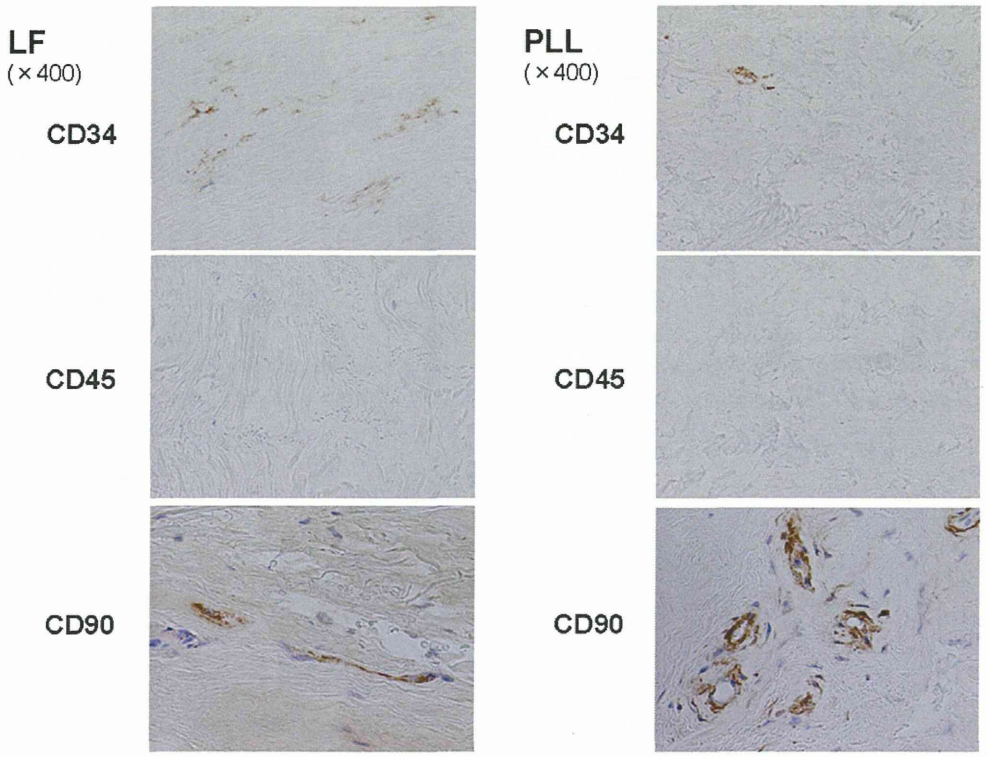

Fig. 4. Immunohistochemical staining of spinal ligament sections with CD34, CD45 and CD90. Typical images were shown. LF: ligamentum flavum, PLL; posterior longitudinal ligament.

Unfortunately, the mechanisms leading to hypertrophy and ossification remain unclear. We hypothesized that MSCs from human spinal ligaments contribute to pathogenic hypertrophy or ossification, but also play important roles in developing and maintaining mesenchymal tissues. Reportedly, aberrant stem cell differentiation can contribute to matrix degeneration and ectopic ossification in patellar tendons of rats [4,5,16] and onset of fibrodysplasia ossificans progressiva [3]. Current data also shows that the committing MSCs to a desired differentiation state is a major requirement and challenge for tissue repair strategies [26]. Determining the roles of stem cells in spinal disease pathogenesis—particularly LSCS, OPLL and OLF – is important for development of therapeutic strategies. Isolation of MSCs from human spinal ligaments, and their localization *in situ*, may thus identify new targets for investigating these diseases.

In conclusion, we have demonstrated, for the first time, the isolation of MSCs from human spinal ligaments and their localization *in situ*. Analyzing the mechanisms of MSC differentiation in human spinal ligaments and how they commit to a differentiated state may provide insight into the treatment of spinal diseases.

Acknowledgments

We thank Drs. Kanichiro Wada, Yoshihito Yamasaki, Yoshifumi Harada, Chin Shunfu, Kazumasa Ueyama, Naoki Echigoya, Akio Sannohe, Toshihiro Tanaka, Toru Yokoyama, Hirotsugu Omi, Taisuke Nitobe, and Kenji Kowatari for their contributions to sample collection. We also thank Ichiro Sekiya and Takeshi Muneta of the Tokyo Medical and Dental University Section of Orthopaedic Surgery for their valuable suggestions.

References

[1] S. Ferguson, Biomechanics of the Spine, in: N. Boos, M. Aebi (Eds.), Spinal Disorders, Springer Verlag, Berlin Heidelberg, 2008, pp. 41–66.
[2] K.-I. Furukawa, Pharmacological aspect of ectopic ossification in spinal ligament tissues, Pharmacol. Ther. 118 (2008) 352–358.
[3] D. Medici, E.M. Shore, V.Y. Lounev, et al., Conversion of vascular endothelial cells into multipotent stem-like cells, Nat. Med. 16 (2010) 1400–1406.
[4] Y.F. Rui, P.P. Lui, L.S. Chan, et al., Does erroneous differentiation of tendon-derived stem cells contribute to the pathogenesis of calcifying tendinopathy? Chin. Med. J. (Engl.) 124 (2011) 606–610.
[5] Y.F. Rui, P.P. Lui, M. Ni, et al., Mechanical loading increased BMP-2 expression which promoted osteogenic differentiation of tendon-derived stem cells, J. Orthop. Res. 29 (2011) 390–396.
[6] D.J. Prockop, Marrow stromal cells as stem cells for nonhematopoietic tissues, Science 276 (1997) 71–74.
[7] M.F. Pittenger, A.M. Mackay, S.C. Beck, et al., Multilineage potential of adult human mesenchymal stem cells, Science 284 (1999) 143–147.
[8] M. Dominici, K. Le Blanc, I. Mueller, et al., Minimal criteria for defining multipotent mesenchymal stromal cells, The International Society for Cellular Therapy position statement, Cytotherapy 8 (2006) 315–317.
[9] C. De Bari, F. Dell'Accio, P. Tylzanowski, et al., Multipotent mesenchymal stem cells from adult human synovial membrane, Arthritis Rheum. 44 (2001) 1928–1942.
[10] Y. Segawa, T. Muneta, H. Makino, et al., Mesenchymal stem cells derived from synovium, meniscus, anterior cruciate ligament, and articular chondrocytes share similar gene expression profiles, J. Orthop. Res. 27 (2009) 435–441.
[11] Y. Sakaguchi, I. Sekiya, K. Yagishita, et al., Suspended cells from trabecular bone by collagenase digestion become virtually identical to mesenchymal stem cells obtained from marrow aspirates, Blood 104 (2004) 2728–2735.
[12] Y. Sakaguchi, I. Sekiya, K. Yagishita, et al., Comparison of human stem cells derived from various mesenchymal tissues: superiority of synovium as a cell source, Arthritis Rheum. 52 (2005) 2521–2529.
[13] T. Mochizuki, T. Muneta, Y. Sakaguchi, et al., Higher chondrogenic potential of fibrous synovium- and adipose synovium-derived cells compared with subcutaneous fat-derived cells: distinguishing properties of mesenchymal stem cells in humans, Arthritis Rheum. 54 (2006) 843–853.
[14] A. Nimura, T. Muneta, H. Koga, et al., Increased proliferation of human synovial mesenchymal stem cells with autologous human serum: comparisons with bone marrow mesenchymal stem cells and with fetal bovine serum, Arthritis Rheum. 58 (2008) 501–510.
[15] S. Wakitani, K. Imoto, T. Yamamoto, et al., Human autologous culture expanded bone marrow mesenchymal cell transplantation for repair of cartilage defects in osteoarthritic knees, Osteoarthritis Cartilage 10 (2002) 199–206.
[16] P.P. Yee Lui, Y.M. Wong, Y.F. Rui, et al., Expression of chondro-osteogenic BMPs in ossified failed tendon healing model of tendinopathy, J. Orthop. Res. 29 (2011) 816–821.
[17] I. Sekiya, B.L. Larson, J.R. Smith, et al., Expansion of human adult stem cells from bone marrow stroma: conditions that maximize the yields of early progenitors and evaluate their quality, Stem cells 20 (2002) 530–541.

[18] I. Sekiya, B.L. Larson, J.T. Vuoristo, et al., Adipogenic differentiation of human adult stem cells from bone marrow stroma, MSCs, J. Bone Miner. Res. 19 (2004) 256–264.
[19] I. Sekiya, B.L. Larson, J.T. Vuoristo, et al., Comparison of effect of BMP-2, -4, and -6 on in vitro cartilage formation of human adult stem cells from bone marrow stroma, Cell Tissue Res. 320 (2005) 269–276.
[20] S. Tanaka, H. Kudo, T. Asari, et al., P2Y1 transient overexpression induced mineralization in spinal ligament cells derived from patients with ossification of the posterior longitudinal ligament of the cervical spine, Calcif. Tissue Int. 88 (2011) 263–271.
[21] A.I. Caplan, Why are MSCs therapeutic? New data: new insight, J. Pathol. 217 (2009) 318–324.
[22] Z. Li, C. Liu, Z. Xie, et al., Epigenetic dysregulation in mesenchymal stem cell aging and spontaneous differentiation, PLoS ONE 6 (2011) e20526.
[23] A.I. Caplan, All MSCs are pericytes? Cell Stem Cell 3 (2008) 229–230.
[24] Y. Bi, D. Ehirchiou, T.M. Kilts, et al., Identification of tendon stem/progenitor cells and the role of the extracellular matrix in their niche, Nat. Med. 13 (2007) 1219–1227.
[25] M. Yoshida, K. Shima, Y. Taniguchi, et al., Hypertrophied ligamentum flavum in lumbar spinal canal stenosis, pathogenesis and morphologic and immunohistochemical observation, Spine (Phila Pa 1976) 17 (1992) 1353–1360.
[26] A. Dickhut, K. Pelttari, P. Janicki, et al., Calcification or dedifferentiation: requirement to lock mesenchymal stem cells in a desired differentiation stage, J. Cell. Physiol. 219 (2009) 219–226.

JOURNAL OF NEUROTRAUMA 28:1–12 (XXXX 2011)

DOI: 10.1089/neu.2011.1919

Rapamycin Promotes Autophagy and Reduces Neural Tissue Damage and Locomotor Impairment after Spinal Cord Injury in Mice

Akira Sekiguchi,[1] Haruo Kanno,[1,2] Hiroshi Ozawa,[1] Seiji Yamaya,[1] and Eiji Itoi[1]

Abstract

The mammalian target of rapamycin (mTOR) is a serine/threonine kinase that negatively regulates autophagy. Rapamycin, an inhibitor of mTOR signaling, can promote autophagy and exert neuroprotective effects in several diseases of the central nervous system (CNS). In the present study, we examined whether rapamycin treatment promotes autophagy and reduces neural tissue damage and locomotor impairment after spinal cord injury (SCI) in mice. Our results demonstrated that the administration of rapamycin significantly decreased the phosphorylation of the p70S6K protein and led to higher expression levels of LC3 and Beclin 1 in the injured spinal cord. In addition, neuronal loss and cell death in the injured spinal cord were significantly reduced in the rapamycin-treated mice compared to the vehicle-treated mice. Furthermore, the rapamycin-treated mice showed significantly higher locomotor function in Basso Mouse Scale (BMS) scores than did the vehicle-treated mice. These results indicate that rapamycin promoted autophagy by inhibiting the mTOR signaling pathway, and reduced neural tissue damage and locomotor impairment after SCI. The administration of rapamycin produced a neuroprotective function at the lesion site following SCI. Rapamycin treatment may represent a novel therapeutic strategy after SCI.

Key words: autophagy; Beclin 1; LC3; mTOR; rapamycin; SCI

Introduction

RAPAMYCIN is a macrolide antibiotic that was first developed as an antifungal agent. Rapamycin is known to be a specific inhibitor of the mammalian target of rapamycin (mTOR) (Ravikumar et al., 2004; Schmelzle and Hall, 2000). Rapamycin binds to the cytosolic protein FK-binding protein 12 (FKBP12). The rapamycin–FKBP12 complex inhibits mTOR, preventing phosphorylation of p70S6K and 4EBP1 (Vignot et al., 2005). Consequently, the inhibition of mTOR by rapamycin promotes autophagy (Kamada et al., 2004; Klionsky and Emr, 2000; Schmelzle and Hall, 2000; Wang and Klionsky, 2003).

Autophagy is an intracellular catabolic mechanism for the degradation of cytoplasmic constituents in the autophagosomal–lysosomal pathway (Mizushima, 2004). This mechanism plays an important role in homeostasis and it is defective in certain diseases (Hara et al., 2006; Liang et al., 1999; Rubinsztein et al., 2005; Shintani and Klionsky, 2004). Autophagy eliminates and recycles long-lived proteins and unwanted damaged organelles in a cell during development and under stress conditions (Levine and Klionsky, 2004; Shintani and Klionsky, 2004). It has been reported that autophagy is also important for normal cell growth, differentiation, and survival (Reggiori and Klionsky, 2002; Schmelzle and Hall, 2000).

Recent studies demonstrated that rapamycin treatment enhances autophagy and rescues neuronal cells in several neurodegenerative diseases such as Huntington's disease and Parkinson's disease (Malagelada et al., 2010; Ravikumar et al., 2004). In such neurodegenerative diseases, induction of autophagy by rapamycin enhances the clearance of a wide range of aggregation-prone proteins and reduces their toxicity (Berger et al., 2006; Webb et al., 2003). Previous studies demonstrated that the activity of autophagy was increased in damaged neural tissue after traumatic brain injury and cerebral ischemia (Bigford et al., 2009; Diskin et al., 2005; Rami et al., 2008). Administration of rapamycin enhances the autophagic activity and reduces neural tissue damage after traumatic brain injury and neonatal hypoxia–ischemia

[1]Department of Orthopaedic Surgery, Tohoku University School of Medicine, Sendai, Japan.
[2]The Miami Project to Cure Paralysis, University of Miami, Miami, Florida.

induced brain injury (Carloni et al., 2008; Erlich et al., 2007a). Several studies also showed that the enhancement of autophagy can reduce apoptosis in damaged neural tissue of the central nervous system (CNS) (Carloni et al., 2008; Pan et al., 2008). Therefore, the promotion of autophagy using rapamycin is considered to provide a neuroprotective function in the CNS.

We previously reported that autophagic activity was significantly increased in damaged neural tissue after spinal cord injury (SCI) (Kanno et al., 2009b, 2011). However, the actual function of autophagy in the damaged neural tissue after SCI is still unclear (Kanno et al., 2009c). Furthermore, whether rapamycin treatment can promote autophagy and induce a neuroprotective function in the damaged neural tissue after SCI remain to be elucidated.

The purpose of the present study was to examine whether rapamycin treatment inhibits the mTOR signaling pathway and promotes autophagy after SCI, using a spinal cord contusion model in mice. We also examined whether rapamycin treatment reduces neural tissue damage such as demyelination, neuronal loss, and cell death, and improves locomotor recovery following SCI.

We show here that rapamycin treatment significantly enhanced autophagic activity by inhibiting mTOR in the injured spinal cord. Furthermore, rapamycin significantly reduced neural tissue damage and improved locomotor function after SCI. Therefore, administration of rapamycin may represent a novel therapeutic strategy after SCI.

Methods

Animals

All experimental procedures were approved by the Institutional Animal Care and Use Committee of Tohoku University. All efforts were made to minimize the number of animals used and to decrease the suffering of the animals used in the study. A total of 58 adult female C57BL/6J mice (10–12 weeks old; Charles River, Japan Inc., Yokohama, Japan) were used in this study. Four or five animals were used for each experimental group at each time point. The mice were housed three or four per cage and kept at a temperature of 24°C with free access to water and food before and after surgery.

Spinal cord contusion injury

The mice were anesthetized with 1.25% halothane in an oxygen/nitrous oxide (30/70%) gas mixture. During surgery, the rectal temperature was monitored and maintained at 37.0 ± 0.5°C by a heating pad. The skin above the vertebral column was shaved and cleaned with antiseptic. A 15-mm mid-line skin incision was made, and the laminae of the T8–T12 vertebrae were exposed. A laminectomy was performed at T10, exposing the dorsal cord surface with the dura intact. The vertebral column was stabilized with angled clamps attached to the T8 and T12 transverse processes. A SCI was induced by a modified New York University Impactor (Basso et al., 1996; Gruner, 1992; Hashimoto et al., 2007; Kanno et al., 2009a; Kim et al., 2001; Okada et al., 2004). A 10 g rod (tip diameter: 1.5 mm) was dropped from 3 mm onto the T10 segment. The impact rod was removed immediately after injury. The muscles and skin were closed in layers. Bladders were expressed twice a day until spontaneous voiding began. The sham-operated animals received the same surgical procedures, but no impact injury was sustained.

Rapamycin preparation and treatment

Rapamycin (Calbiochem) was dissolved in dimethyl sulfoxide (DMSO) (25 mg/mL) and further diluted in 0.5 mL aqueous solution containing 5% polyethylene glycol 400 and 5% Tween 80 immediately before injection. At 4 h after SCI, mice in the rapamycin treatment group were injected intraperitoneally with rapamycin at a dose of 1 mg/kg body weight. Control animals were injected with an equivalent volume of the vehicle.

Behavioral analysis

To evaluate the functional consequences of SCI, a locomotor rating test using the Basso Mouse Scale (BMS) was performed (Basso et al., 2006; Engesser-Cesar et al., 2005). This scale was developed specifically for mice because the characteristics of locomotor recovery are different in mice than in rats. We also analyzed the BMS subscore, because some animals can show improvements in specific aspects of locomotion that do not follow a typical pattern of recovery, and therefore are not reflected in any change in the overall score on the BMS (Basso et al., 2006). Before surgery, the mice were placed individually in a molded plastic open field for 4 min to assure that all subjects consistently obtained the maximum score. The mice were placed in the open field, and well-trained investigators scored them on the BMS in a blinded manner. The BMS scores were measured at 4 and 24 h, and at 3, 7, 14, 21, 28, 35, and 42 days after SCI.

Western blot analysis

The mice were killed at 24 h or 3 days after SCI, and their spinal cords were removed. The spinal cords were homogenized in lysis buffer containing 50 mM Tris HCl (pH 7.6), 20 mM MgCl2, 150 mM NaCl, 0.5% Triton-X, 5 units/mL aprotinin, 5 μg/mL leupeptin, 5 μg/mL pepstatin, 1 mM benzamidine, and 1 mM phenylmethylsulfonyl fluoride. The debris was removed by centrifugation, and the protein levels in the lysates were determined with the aid of the Bio-Rad protein assay (Bio-Rad Laboratories, GmbH, Munich, Germany). The proteins in the lysates were separated by SDS–polyacrylamide gel electrophoresis (PAGE) in 15% gels, and then electrophoretically transferred to polyvinylidene difluoride membranes. The membranes were blocked for 1 h in TBST buffer (0.01 M Tris HCl, pH 7.5, 0.15 M NaCl and 0.05% Tween 20) containing 3% milk, and incubated with rabbit anti-phospho-p70S6K antibody (1:1000; Cell Signaling Technology), rabbit anti-LC3 antibody (1:500; MBL) or rabbit anti-Beclin 1 antibody (1:100; Santa Cruz Biotechnology) diluted in TBST buffer overnight at 4°C. The membranes were washed three times and incubated with secondary antibody linked to horseradish peroxidase (1:1000; Invitrogen) for 1 h at room temperature. The immunoreactive bands were developed using enhanced chemiluminescence reagents (Amersham Corp.) and digitalized by the LAS-1000 Pro (FUJIFILM, Tokyo, Japan). The band densities were quantified using a scanned densitometric analysis and the Image J 1.42q software program (National Institutes of Health). The quantities of the band densities were normalized to β-tubulin, and thereafter, those quantities

were compared among the rapamycin-treated mice, the vehicle-treated mice and the sham controls.

Tissue preparation

At 3 days and 42 days after SCI, the mice were overdosed with an intraperitoneal injection of 100 mg/kg sodium pentobarbital. The mice were transcardially perfused with normal saline, followed by 4% paraformaldehyde in 0.1 M phosphate-buffered saline (PBS) at pH 7.4. For immunohistochemical staining, the spinal cord segments containing the injured site were collected, post-fixed in the same fixative overnight at 4°C, and embedded in paraffin. Serial 7-μm transverse sections around the injured site were mounted on slides. A total of 9 sequential sections at 250 μm intervals were collected, spanning a 2000 μm length in the spinal cord centered at the epicenter. The sections were used for immunohistochemical staining as described in the next section.

Immunohistochemistry

Immunohistochemical staining for LC3 and Beclin 1 was performed using the sections obtained 3 days after SCI. The sections were de-paraffinized and rehydrated, and then were washed in PBS for 10 min, followed by washing with PBS containing 0.3% Tween for 10 min, and blocking with 3% milk and 5% fetal bovine serum (FBS) in 0.01 M PBS for 2 h. The sections were incubated with rabbit anti-LC3 antibody (1:100; MBL), rabbit anti-Beclin 1 antibody (1:100; Santa Cruz Biotechnology) or mouse anti-NeuN antibody (1:100; Chemicon) diluted in PBS overnight at 4°C. After rinsing with PBS, the sections were incubated with goat anti-rabbit IgG Alexa Fluor 594 secondary antibody (1:500; Molecular Probes) or goat anti-mouse IgG Alexa Fluor 488 secondary antibody (1:500; Molecular Probes) for 1 h at room temperature. The sections were mounted with Vectashield containing DAPI to label the nuclei (Vector Laboratories). In each experiment, the sections were stained at the same time.

Counting of LC3-positive cells and Beclin 1-positive cells

Each section was scanned using a laser microscope (BX 51; Olympus, Tokyo, Japan) following the immunochemical staining of LC3 and Beclin 1. The scanned image of the transverse section was displayed on a monitor with a grid using the Photoshop Elements Software Program Version 6.0 (Adobe, CA). Then LC3-positive cells and Beclin 1-positive cells in the section were counted using a manual counter. The LC3-positive cells were defined as those displaying punctate LC3 fluorescent dots (Kabeya et al., 2000; Rami et al., 2008). The LC3-positive cells and the Beclin 1-positive cells were counted in the sections at the epicenter, and on the 250 μm and 500 μm rostral and caudal sides. The sum of the numbers in the five sections was compared among the rapamycin-treated mice, the vehicle-treated mice, and the sham controls.

White matter staining

The serial 7-μm transverse sections cut at 250 μm intervals around the epicenter 42 days after SCI were stained with luxol fast blue for myelin. The section with the least amount of luxol fast blue stain was selected as the lesion epicenter. A total of nine sequential sections spanning 2000 μm of spinal cord length, which included four sections both rostral and caudal to the section at the epicenter, were assessed. The images of the stained sections were captured by a digital photographic camera, and the spared white matter area of the spinal cord was analyzed using the Image J 1.42q software program. After performing the luxol fast blue staining, the spared white matter appeared dark blue and isocellular, as seen in healthy neuronal tissue. The damaged or degenerated white matter appeared to be either blanched or replaced by scar tissue having clusters of cells with prominent basophilic nuclei (Bao et al., 2011; Joshi and Fehlings, 2002; Steward et al., 1999). We analyzed the spared white matter area in the rapamycin-treated and the vehicle-treated mice.

Counting of NeuN-positive cells

After the immunohistochemical staining of NeuN as described previously, each section was scanned using a microscope (BX 51; Olympus, Tokyo, Japan). To investigate neuronal loss in the SCI, the number of NeuN-positive cells in each section 42 days after injury was counted. The NeuN-positive cells were defined as cells double labeled with NeuN and DAPI. The section at the epicenter, and 250 μm rostral and caudal sections were chosen for each animal. The cell counting procedure was the same as that described previously. The sum of the numbers in the three sections was compared between the rapamycin-treated and the vehicle-treated mice.

Counting of TUNEL-positive cells

To detect DNA fragmentation caused by cell death in the injured spinal cord, terminal deoxynucleotidyl transferase-mediated dUTP nick end labeling (TUNEL) staining was applied using the In Situ Cell Death Detection Kit (Roche, Mannheim, Germany) for the transverse sections obtained at 3 days after injury. The labeled sections at the lesion epicenter and the sites 250 μm caudal and rostral to the lesion were scanned with a BX 51 microscope. The number of TUNEL-positive cells in each section was counted. The TUNEL-positive cells were defined as cells double labeled with TUNEL and DAPI. The cell counting procedure was the same as that described previously. The sum of the numbers in the three sections for each animal was calculated and compared between the rapamycin-treated and the vehicle-treated mice.

Statistical analysis

Significant differences in the number of LC3-positive cells, the number of Beclin 1-positive cells, the number of TUNEL-positive cells, the band densities obtained from the Western blot analyses, and in the spared white matter area, were analyzed using the unpaired t test. The significance of any differences in the BMS scores at each time point was determined by Mann–Whitney's U test. In all analyses, a p value < 0.05 was considered to be statistically significant. All statistical analyses were performed using the GraphPad Prism 5.0a software program (GraphPad Software, Inc. La Jolla, CA).

Results

BMS locomotor scores

To evaluate the effect of rapamycin treatment on locomotor recovery after SCI, the BMS total scores and subscores were

measured for 6 weeks (Fig. 1A, B). The total BMS scores in the rapamycin-treated mice and in the vehicle-treated mice increased after 4 h and reached a plateau at 28 days after injury. The averages of the total BMS scores were consistently higher in the rapamycin-treated mice than in the vehicle-treated mice from 14 days to 42 days after injury. The rapamycin-treated mice had significantly higher total BMS scores than the vehicle-treated mice from 21 days to 42 days. At 42 days after injury, the total BMS scores of the rapamycin-treated mice were 7–9 (8.4 ± 0.4). Except for one rapamycin-treated mouse with a BMS score of 7, the other four rapamycin-treated mice consistently achieved coordinated plantar stepping with normal trunk stability or with mild trunk instability at 42 days. On the other hand, the BMS scores of the vehicle-treated mice were 5–8 (6.8 ± 0.5). Four out of 5 vehicle-treated mice did not keep their paws parallel when stepping, or they showed severe trunk instability such as leaning, waddling, or near collapse of the hindlimbs.

The BMS subscores of both the rapamycin-treated mice and the vehicle-treated mice increased after 24 h and reached a plateau at 28 days. The average subscores were consistently higher in the rapamycin-treated mice than in the vehicle-treated mice from 14 days to 42 days. The BMS subscore was significantly higher in the rapamycin-treated mice than in the vehicle-treated mice from 14 days to 42 days after injury.

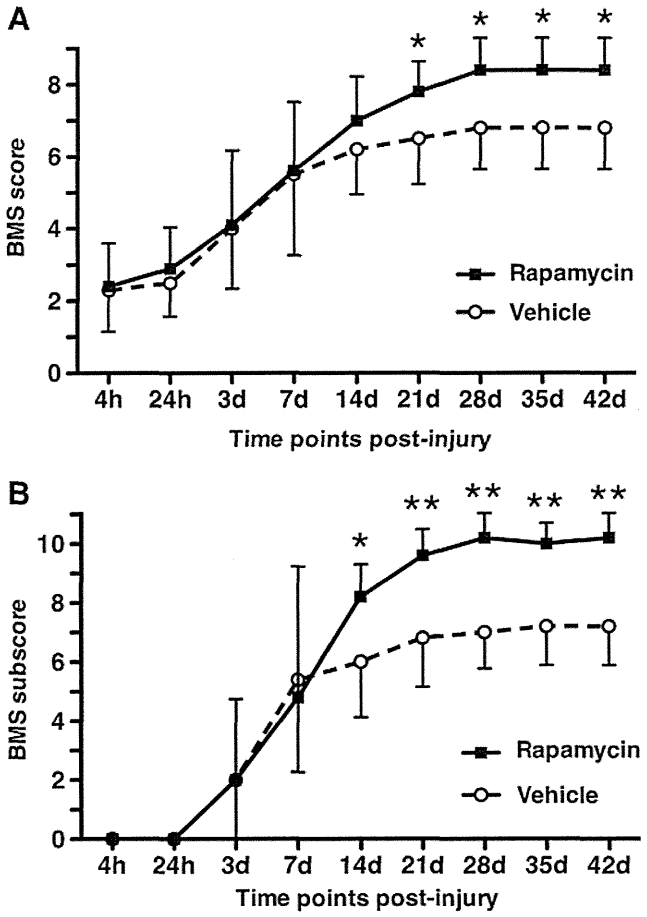

FIG. 1. Locomotor recovery after SCI in vehicle-treated mice and rapamycin-treated mice. The BMS scores **(A)** and BMS subscores **(B)** were determined from 4 h to 42 days after injury. **(A)** The BMS scores were consistently higher in the rapamycin-treated mice than in the vehicle-treated mice from days 14 to 42. The rapamycin-treated mice had significantly higher BMS scores than the vehicle-treated mice from days 21 to 42. **(B)** The BMS subscores were also consistently higher in the rapamycin-treated mice than in the vehicle-treated mice from days 14 to 42. The rapamycin-treated mice had significantly higher BMS scores than the vehicle-treated mice from days 14 to 42. The values are the means ± SD (*$p < 0.05$, **$p < 0.01$, $n = 5$ per each group).

Phosphorylation of p70S6K

To examine the effectiveness of the rapamycin treatment on the mTOR signaling pathway in the mice, the phosphorylation of p70S6K was evaluated by Western blot analysis. The phosphorylated p70S6K protein was decreased in the rapamycin-treated mice compared with the vehicle-treated mice and the sham controls at 24 h and 3 days after injury (Fig. 2A). Based on the analysis of the band density, the level of phosphorylated p70S6K was significantly lower in the rapamycin-treated mice (2.318 ± 0.866) than in the vehicle-treated mice (8.773 ± 1.083) and in the sham controls (10.000 ± 1.794) ($p = 0.002$ and 0.005, respectively) at 24 h (Fig. 2B). The level of phosphorylated p70S6K at 3 days did not show any statistical differences among the three groups.

Immunohistochemical and Western blot analyses of LC3 expression

To investigate the activation of autophagy after rapamycin treatment, immunohistochemical staining of LC3 was

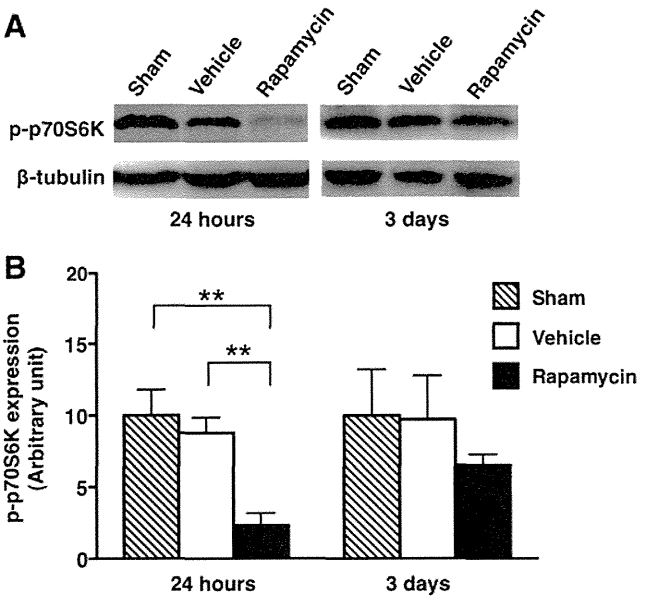

FIG. 2. The expression of phosphorylated p70S6K in sham control, vehicle-treated mice and rapamycin-treated mice. **(A)** Western blot analysis of phosphorylated p70S6K and β-tubulin protein expression levels. **(B)** A quantitative analysis of Western blots showed that the levels of phosphorylated p70S6K in the rapamycin-treated mice were significantly lower than in the vehicle-treated mice and the sham controls at 24 h ($p = 0.002$ and 0.005, respectively). The quantities of the band densities were normalized to β-tubulin. The values are the means ± SD (**$p < 0.01$, $n = 4$ per each group).

performed, and the number of LC3-positive cells was counted. The cells expressing LC3 were increased in the rapamycin-treated mice and in the vehicle-treated mice compared with the sham controls (Fig. 3A–I,S). The population of cells expressing LC3 in the rapamycin-treated mice was obviously higher than that in the vehicle-treated mice. Higher magnification revealed that the LC3-expressing cells displayed punctate LC3 dots that were located in the cytoplasm (Fig. 3J–R). The number of LC3-positive cells was significantly increased in the vehicle-treated mice and the rapamycin-treated mice compared with the sham controls ($p = 0.012$ and < 0.001, respectively). In addition, the number of LC3-positive cells in the rapamycin-treated mice was significantly higher than in the vehicle-treated mice ($p = 0.018$) (Fig. 3T).

In the Western blot analysis, the expression of LC3-II protein was increased in the rapamycin-treated mice compared with the vehicle-treated mice and the sham controls (Fig. 4A). In the analysis of the band density, the level of LC3-II expression was significantly higher in the rapamycin-treated mice (7.274 ± 0.783) and vehicle-treated mice (4.717 ± 0.532) than in the sham controls (1.000 ± 0.380) ($p = 0.002$ and 0.001, respectively). In addition, the LC3-II expression was significantly higher in the rapamycin-treated mice than in the vehicle-treated mice ($p = 0.035$) (Fig. 4B).

Immunohistochemical and Western blot analyses of Beclin 1 expression

To analyze the autophagic activity, we also performed immunohistochemistry for Beclin 1, and counted Beclin 1-positive cells. The Beclin 1 expressing cells were clearly increased in the rapamycin-treated mice and in the vehicle-treated mice compared with the sham controls (Fig. 5A–I,S). The number of Beclin 1-positive cells was significantly increased in the rapamycin-treated mice and the vehicle-treated mice compared with the sham controls ($p = 0.005$ and < 0.001, respectively) (Fig. 5T).

In the Western blot analysis, the expression of Beclin 1 protein was significantly increased in the rapamycin-treated mice and the vehicle-treated mice compared with in the sham controls (Fig. 6A, B). In the analysis of the band density, the level of Beclin 1 expression was significantly higher in the rapamycin-treated mice (7.411 ± 0.882) and vehicle-treated mice (6.506 ± 0.609) than in the sham controls (1.000 ± 0.594) ($p < 0.001$ and 0.001, respectively). In addition, the Beclin 1 expression in the rapamycin-treated mice was relatively

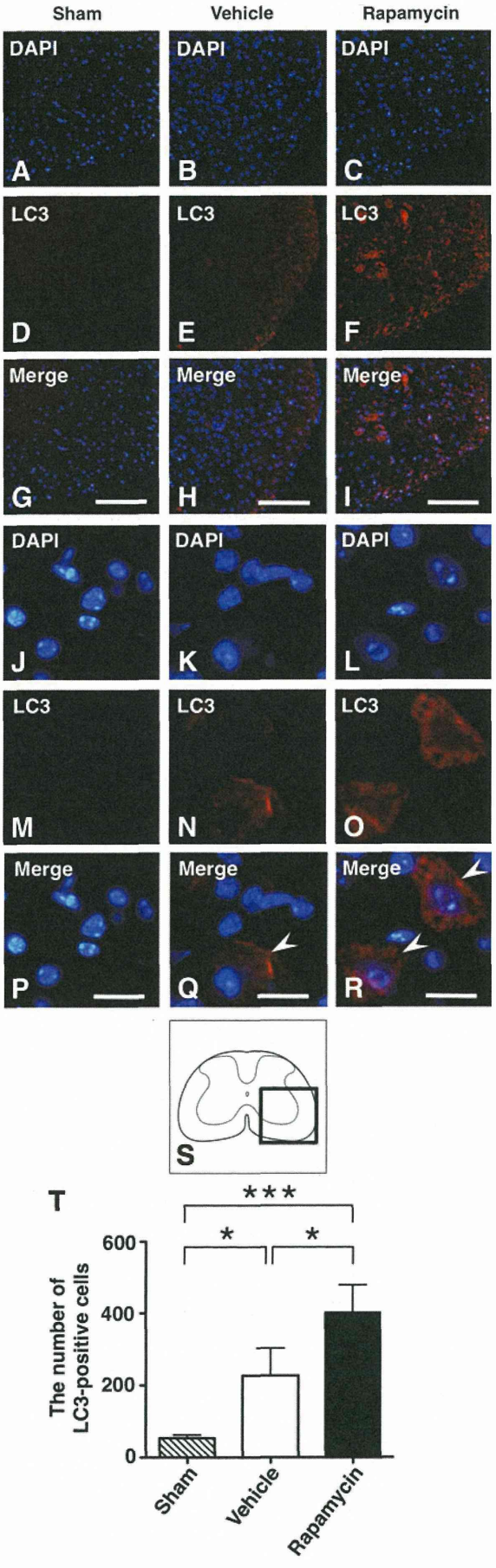

FIG. 3. Immunohistochemical staining of LC3 in sham control, vehicle-treated mice and rapamycin-treated mice. **(A–I)** Representative spinal cord sections from the epicenter show that the population of LC3-positive cells was increased in the rapamycin-treated mice compared with the vehicle-treated mice and the sham controls. Scale bars = 100 μm. **(J–R)** On higher magnification, LC3-positive cells were observed in the rapamycin-treated mice and the vehicle-treated mice (Arrowheads in **Q** and **R**). Scale bars = 10 μm. **(S)** The schematic drawing illustrates the location of the micrographs. **(T)** The number of LC3-positive cells was significantly higher in the rapamycin-treated mice than in the vehicle-treated mice and the sham controls ($p = 0.018$ and < 0.001, respectively). The values are the means ± SD (*$p < 0.05$, ***$p < 0.001$, $n = 4$ per each group).

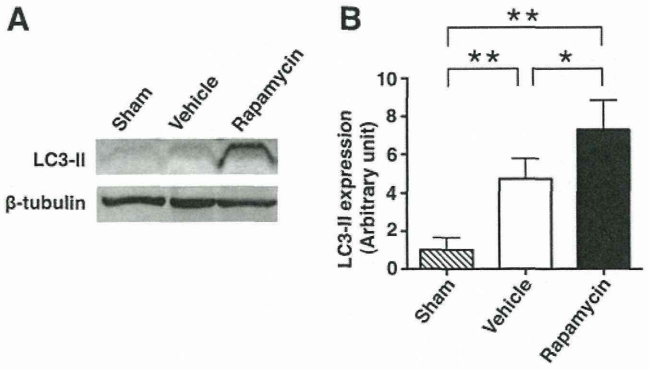

FIG. 4. The expression of LC3-II in sham controls, vehicle-treated mice and rapamycin-treated mice. **(A)** A Western blot analysis of LC3-II and β-tubulin protein expression. **(B)** A quantitative analysis of Western blots showed that the levels of LC3-II in the rapamycin-treated mice were significantly higher than in the vehicle-treated mice and the sham controls ($p=0.035$ and 0.001, respectively). The quantities of the band densities were normalized to β-tubulin. The values are the means ± SD (*$p<0.05$, **$p<0.01$, $n=4$ per group).

higher, but not significantly so, than that in the vehicle-treated mice.

Areas of spared white matter

To investigate the differences in the amounts of demyelination after the injury, the spared white matter areas were compared between the rapamycin-treated and the vehicle-treated mice using luxol fast blue staining. The areas of spared white matter in the rapamycin-treated mice were obviously larger than in the vehicle-treated mice, as indicated by the luxol fast blue staining of the sections around the epicenter (Fig. 7A,B). The white matter area was more preserved in the rapamycin-treated mice than in the vehicle-treated mice, especially in the dorsal side of the spinal cord (Fig. 7B). In quantitative analysis of the spared white matter area, the averages of spared white matter area in the rapamycin-treated mice were not significantly but consistently larger than in the vehicle-treated mice at >500 μm rostral and caudal sides from the epicenter (Fig. 7C).

The number of NeuN-positive cells

To investigate loss of neural cells after injury, the number of NeuN-positive cells was compared between the vehicle and

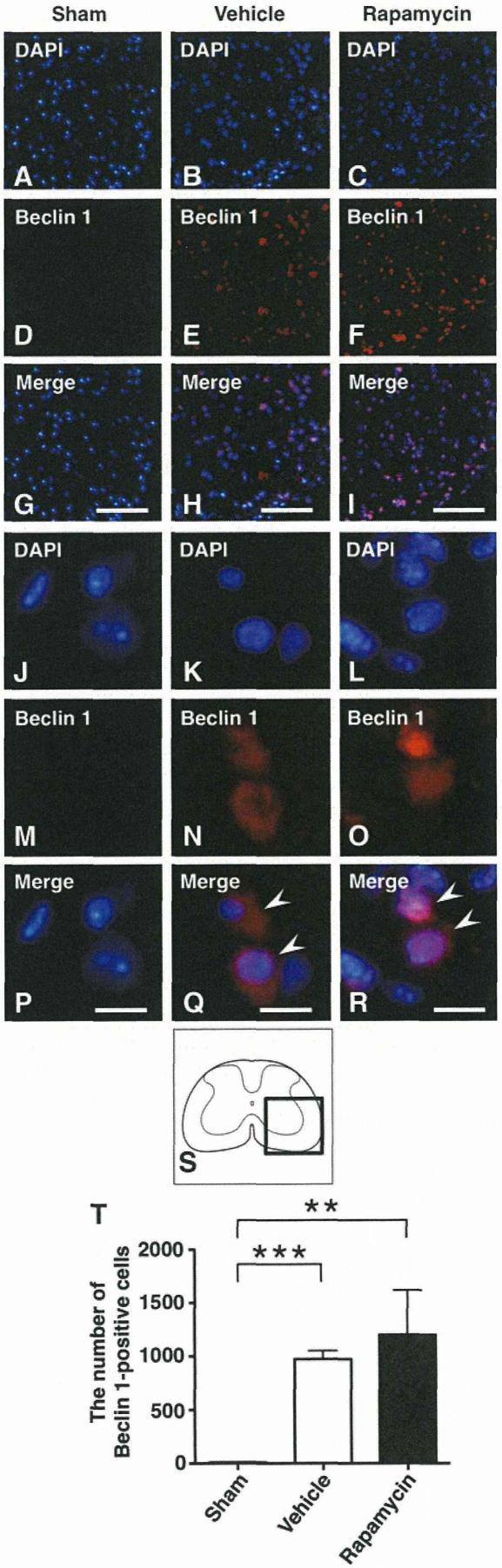

FIG. 5. Immunohistochemical staining of Beclin 1 in sham control, vehicle-treated mice and rapamycin-treated mice. **(A–I)** Representative spinal cord sections from the epicenter show that the population of the Beclin 1-positive cells was increased in the rapamycin-treated mice and the vehicle-treated mice compared with the sham controls. Scale bars = 100 μm **(G–I)**. On higher magnification, Beclin 1-positive cells were observed in the rapamycin-treated mice and the vehicle-treated mice (Arrowheads in **Q** and **R**). Scale bars = 10 μm. **(S)** The schematic drawing illustrates the location of the micrographs. **(T)** The number of Beclin 1-positive cells was significantly higher in the rapamycin-treated mice and the vehicle-treated mice than in the sham controls ($p=0.005$ and <0.001, respectively). The values are the means ± SD (**$p<0.01$, ***$p<0.001$, $n=4$ per each group).

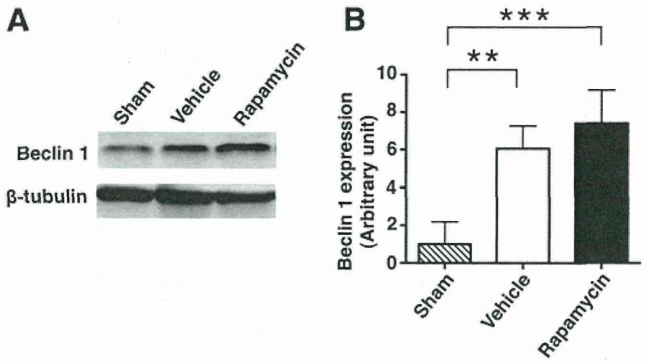

FIG. 6. The expression of Beclin 1 in sham control, vehicle-treated mice and rapamycin-treated mice. **(A)** A Western blot analysis of Beclin 1 and β-tubulin protein expression. **(B)** A quantitative analysis of Western blots showed that the levels of Beclin 1 in the rapamycin-treated mice and the vehicle-treated mice were significantly higher than those in the sham controls ($p<0.001$ and 0.001, respectively). The quantities of the band densities were normalized to β-tubulin. The values are the means ± SD (**$p<0.01$, ***$p<0.001$, $n=4$ per each group).

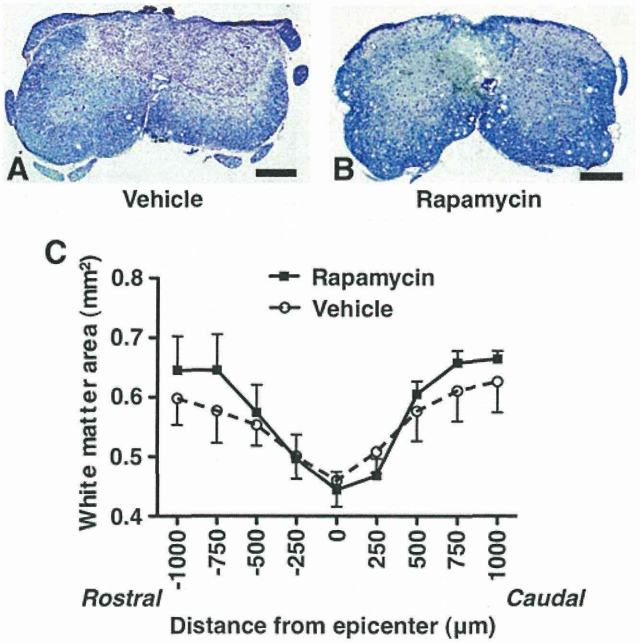

FIG. 7. White matter sparing in the vehicle-treated mice and rapamycin-treated mice at 42 days after SCI. Representative spinal cord sections at the 750 μm rostral side from the epicenter showed that the spared white matter area was relatively smaller in the vehicle-treated mice **(A)** than in the rapamycin-treated mice **(B)**. Scale bars = 500 μm. **(C)** The spared white matter area from the epicenter to 2000 μm on the rostral and caudal side was compared in the vehicle-treated mice and the rapamycin-treated mice. The areas of spared white matter were not significantly, but were consistently larger in the rapamycin-treated mice than in the vehicle-treated mice at >500 μm rostral and caudal from the epicenter. The values are the means ± SEM ($n=4$ per each group). Color image is available online at www.liebertonline.com/neu

the rapamycin-treated mice by immunohistochemical staining. The NeuN-positive cells were sparsely observed at the epicenter in the vehicle-treated mice. In contrast, the rapamycin-treated mice showed a higher number of NeuN-positive cells compared with the vehicle-treated mice (Fig. 8A–M). The number of NeuN-positive cells in the rapamycin-treated mice was significantly higher than those in the vehicle-treated mice at 42 days ($p=0.012$) (Fig. 8N).

The number of TUNEL-positive cells

To investigate the effect of rapamycin on cell death after SCI, we performed TUNEL staining, and the number of TUNEL-positive cells was compared between the vehicle- and the rapamycin-treated mice. In the TUNEL staining of sections obtained at 3 days after injury, the TUNEL-positive cells were obviously decreased in the rapamycin-treated mice compared with the vehicle-treated mice (Fig. 9A–M). When the TUNEL-positive cells were counted, the number of TUNEL-positive cells was significantly lower in the rapamycin-treated mice compared to the vehicle-treated mice ($p=0.008$) (Fig. 9N).

Discussion

In the present study, we demonstrated that the administration of rapamycin significantly decreased the phosphorylation of p70S6K protein and led to higher expressions of LC3 and Beclin 1 in the injured spinal cord. In addition, neuronal loss and cell death in the injured spinal cord were significantly more reduced in the rapamycin-treated mice than in the vehicle-treated mice. Furthermore, the rapamycin-treated mice showed significantly higher locomotor function in BMS scores than did the vehicle-treated mice after SCI. These results demonstrated that the administration of rapamycin promoted autophagy by inhibiting mTOR signaling pathway and reduced neural tissue damage and locomotor impairment after SCI. The present study indicated that rapamycin treatment had a neuroprotective effect at the lesion site following SCI.

Previous studies demonstrated that rapamycin treatment inhibits the mTOR signaling pathway and activates autophagy in several neurodegenerative diseases (Pan et al., 2008; Ravikumar et al., 2004). Additionally, rapamycin enhanced autophagic activity after traumatic brain injury and neonatal hypoxia–ischemia induced brain injury (Carloni et al., 2008; Erlich et al., 2007a). These data indicate that rapamycin promotes autophagy by inhibiting mTOR in the CNS. In the present study, rapamycin treatment significantly reduced the phosphorylation of p70S6K protein in the injured spinal cord. The reduction of phosphorylated p70S6K indicated that administration of rapamycin actually inhibited mTOR signaling after SCI. Our results also showed that rapamycin treatment induced upregulation of LC3 and Beclin 1 expression in the damaged neural tissue after SCI. These findings demonstrated that rapamycin promoted autophagy by inhibiting mTOR pathway at the lesion site following SCI.

The autophagic activity is regulated by various molecular factors including mTOR, Beclin 1, Bcl family, DRAM, p53, and NF-κB (Maiuri et al., 2007; Scarlatti et al., 2009). Previous research has suggested that Beclin 1 regulates not only the autophagic activity, but also the cell death mechanism (Maiuri et al., 2007). Beclin 1 interacts with Bcl-2, which is known to be an anti-apoptotic protein (Erlich et al., 2007b). Therefore, the

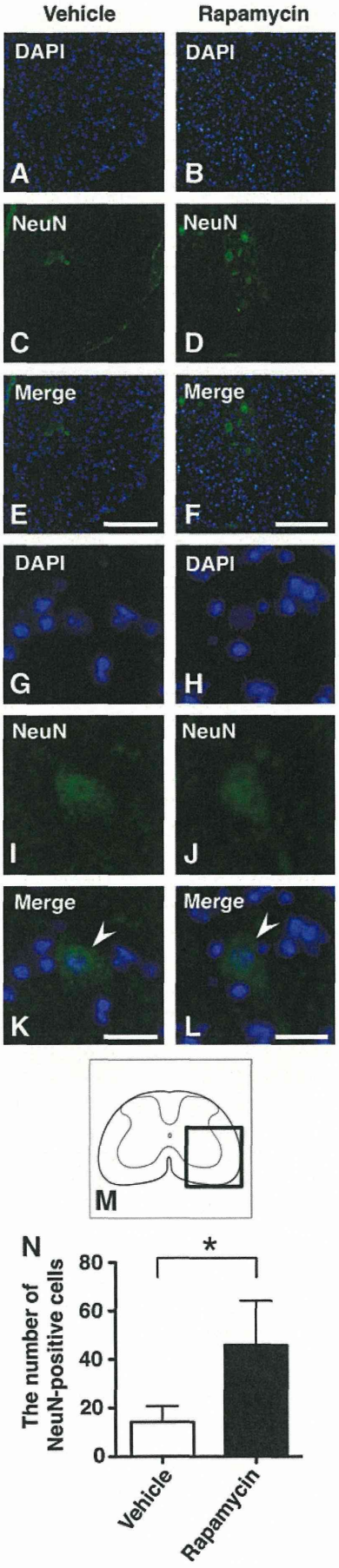

level of Beclin 1 expression may not directly indicate the level of autophagic activity. In this study, the expression of LC3, a marker of autophagy, significantly increased due to the administration of rapamycin after SCI. However, the increase in the Beclin 1 expression after the rapamycin treatment was not statistically significant. These findings suggested that the activation of autophagy after rapamycin treatment therefore did not directly indicate the upregulation of Beclin 1 expression after SCI.

The inhibition of mTOR by rapamycin can cause either beneficial or detrimental effects, depending upon the disease model and timing. Previous studies suggested that rapamycin treatment aggravated renal ischemia/reperfusion injury (Gonçalves et al., 2007; Lui et al., 2006). Rapamycin blocks the cardioprotective effect of ischemic or pharmacological preconditioning for myocardial infarction (Jonassen et al., 2001; Kis et al., 2003). On the other hand, rapamycin treatment had a cytoprotective effect, including reduction of infarct size and decreasing cell death caused by myocardial ischemia/reperfusion injury (Khan et al., 2006). The enhancement of autophagy using rapamycin also produces a neuroprotective function in various diseases of the CNS. Previous studies demonstrated that administration of rapamycin rescued neuronal cells in models of Huntington's disease and Parkinson's disease (Malagelada et al., 2010; Ravikumar et al., 2004). Interestingly, rapamycin treatment reduces neural tissue damage after traumatic brain injury and neonatal hypoxia–ischemia induced brain injury (Carloni et al., 2008; Erlich et al., 2007a). In the present study, rapamycin prevented the neuronal loss after SCI. Moreover, the rapamycin-treated mice showed significantly better locomotor recovery in BMS scores. The present study suggested that administration of rapamycin provided a beneficial effect by reducing the neural tissue damage and locomotor impairment following SCI.

Rapamycin has cytoprotective effects that have been attributed to blocking the apoptotic signaling pathway (Carloni et al., 2008; Khan et al., 2006; Pan et al., 2008). It has been suggested that rapamycin enhances the clearance of mitochondria by autophagy, thereby reducing cytosolic cytochrome c release and downstream caspase activation (Ravikumar et al., 2006). Previous studies demonstrated rapamycin to have a cytoprotective function by reducing apoptosis in various disease models. For example, rapamycin treatment significantly reduced the number of TUNEL-positive cells in myocytes in a myocardial ischemia-reperfusion model (Khan et al., 2006). Rapamycin promoted autophagy and inhibited apoptosis in a model of lactacystin-induced neurodegeneration (Pan et al., 2008). Activation of autophagy by rapamycin also reduced the expression of activated

FIG. 8. *Immunohistochemical staining of NeuN in vehicle-treated mice and rapamycin-treated mice at 42 days after SCI.* Representative sections at the epicenter showed that there were fewer NeuN-positive cells in the vehicle-treated mice **(A, C, E)** than in the rapamycin-treated mice **(B, D, F)**. Scale bars = 100 μm. **(G–L)** Magnified images showed NeuN-positive cells (arrowheads). Scale bars = 20 μm. **(M)** The schematic drawing illustrates the location of the micrographs. **(N)** The number of NeuN-positive cells was significantly lower in the vehicle-treated mice than in the rapamycin-treated mice ($p = 0.012$). The values are the means ± SD (*$p < 0.05$, $n = 4$ per each group). Color image is available online at www.liebertonline.com/neu

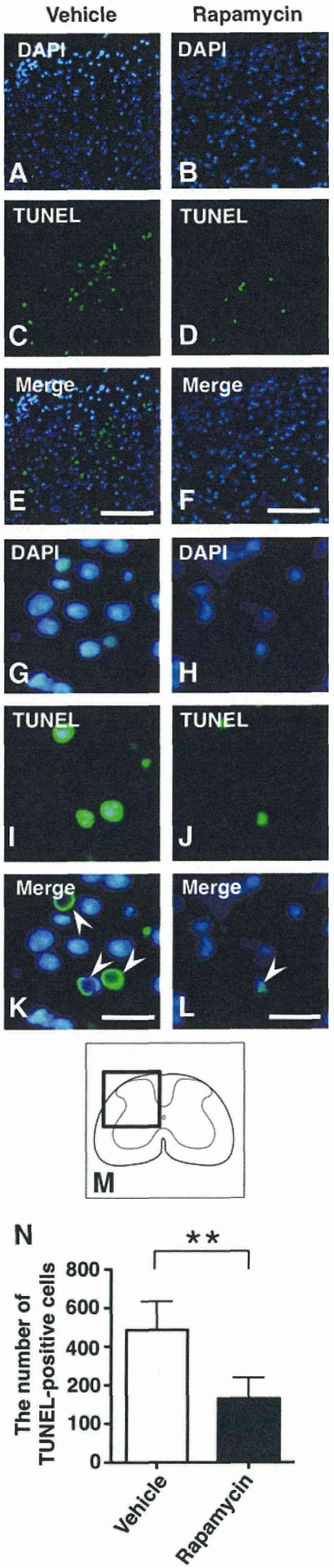

caspase-3 in a model of neonatal hypoxia-ischemia induced brain injury (Carloni et al., 2008). Interestingly, in these disease models of the CNS, the activity of autophagy was upregulated even without the administration of rapamycin and it was further enhanced by rapamycin treatment (Carloni et al., 2008; Pan et al., 2008). These reports suggested that the rapamycin treatment further promoted autophagic activity and reinforced its cytoprotective function to reduce cell death in such diseases of the CNS. In the present study, rapamycin further promoted the activity of autophagy that had been upregulated after SCI. Additionally, the rapamycin treatment significantly reduced the number of TUNEL-positive cells at 3 days after SCI. These findings suggested that rapamycin treatment enhanced the activity of autophagy and thereby prevented cell death in the damaged neural tissue after SCI.

The administration of rapamycin in this study was performed using a single injection at 4 h after SCI. Many previous studies that investigated the pharmacokinetics of rapamycin *in vivo* showed the half-life of rapamycin to be relatively long (33–63 h) (Chen et al., 2007; Napoli et al., 1997). In fact, several reports demonstrated that a single administration of rapamycin could affect the autophagic activity and cell death for >24 h (Carloni et al., 2008; Sheng et al., 2010). In the present study, the single administration of rapamycin at 4 h actually inhibited the phosphorylation of p70S6K in mTOR signaling pathway at 24 h after SCI, and produced a significant reduction in the degree of neuronal loss and cell death. These results indicated the rapamycin treatment at 4 h could reduce the secondary injury that mainly occurs from 24 h to 3 days after the onset of SCI (Beattie et al., 2000; Yong et al., 1998). The present study suggested that the administration of rapamycin produces a cytoprotective effect at the lesion site. Therefore, the administration of rapamycin may represent a novel therapeutic strategy to reduce secondary injury following SCI.

Recent studies have indicated that the inhibition of mTOR by rapamycin can suppress the regeneration of damaged neural tissue. The inhibition of mTOR by rapamycin suppresses growth cone regeneration after axonotomy (Verma et al., 2005). Axonal regeneration activated by the administration of adenosine-5′-triphosphate (ATP) in the injured spinal cord can decrease because of the administration of rapamycin (Hu et al., 2010). Rapamycin reduces the ability of axonal regeneration that was promoted by the deletion phosphatase and tensin homolog (PTEN) in the CNS (Park et al., 2008). These studies suggested that the inhibition of mTOR by rapamycin suppressed new protein synthesis and cell proliferation to promote axonal regeneration. On the other hand, a few reports have indicated that rapamycin could promote a permissive environment for neuroregeneration.

FIG. 9. TUNEL staining in vehicle-treated mice and rapamycin-treated mice at 3 days after SCI. Representative sections at the epicenter showed that there were obviously fewer TUNEL-positive cells in the rapamycin-treated mice **(B, D, F)** than in the vehicle-treated mice **(A, C, E)**. Scale bar = 100 μm. **(G–L)** Magnified images showed TUNEL-positive cells (arrowheads). Scale bars = 20 μm. **(M)** The schematic drawing illustrates the location of the micrographs. **(N)** The number of TUNEL-positive cells was significantly lower in the rapamycin-treated mice than in the vehicle-treated mice ($p = 0.008$). The values are the means ± SD (**$p < 0.01$, $n = 4$ per each group). Color image is available online at www.liebertonline.com/neu